University of Thessaly

School of Engineering

Department of Mechanical Engineering

Laboratory of Materials

Experimental and theoretical study of Hot Cracking phenomena in Laser Beam Welding of 2198 Aluminum Alloy

Author
Efstratios Th. Koufis

Supervisor
Dr. Anna D. Zervaki

Volos 2018

Submitted in partial fulfillment of
the requirements for the Diploma
of Mechanical Engineering

Thesis committee

1^{st} *Member* (Supervisor)	*Dr. Anna D. Zervaki* Lab Teaching Staff, Department of Mechanical Engineering, University of Thessaly
2^{nd} *Member*	*Dr. Spyros A. Karamanos* Professor, Department of Mechanical Engineering, University of Thessaly
3^{rd} *Member*	*Dr. Alexis Th. Kermanidis* Assistant Professor, Department of Mechanical Engineering, University of Thessaly

Ευχαριστίες/Acknowledgments

Αρχικά, θα ήθελα να ευχαριστήσω θερμά την επιβλέπουσα της παρούσας διπλωματικής εργασίας Δρ. Άννα Ζερβάκη για την καθοδήγηση που μου παρείχε αλλά και για την γενικότερη υποστήριξη και εμπιστοσύνη που έδειξε στο πρόσωπο μου κατά τον τελευταίο χρόνο.

Επίσης θα ήθελα να ευχαριστήσω πολύ τους Καθηγητές Κ.Κ. Αλέξη Κερμανίδη και Σπύρο Καραμάνο για τον χρόνο που αφιέρωσαν για την εξέταση της εργασίας μου. Ακόμα, θα ήθελα να ευχαριστήσω την Καθηγήτρια του Αριστοτέλειου Πανεπιστήμιου Θεσσαλονίκης Κα. Ελένη Παυλίδου για την πολύτιμη συνεισφορά της στο πειραματικό κομμάτι των EDX αναλύσεων αλλά και τον Καθηγητή της Σ.Σ.Ε. Κο. Διονύση Μουζάκη για την συνεισφορά του στο κομμάτι της ηλεκτρονικής μικροσκοπίας και των αρχικών EDX αναλύσεων.

Επιπροσθέτως, θα ήθελα να ευχαριστήσω και πάλι την Δρ. Άννα Ζερβάκη αλλά και τον Καθηγητή του Πανεπιστημίου Θεσσαλίας Κο. Γρηγόρη Χαιδεμενόπουλο οι οποίοι μέσω της διδασκαλίας των μαθημάτων τους αλλά και γενικότερα μέσω της δραστηριότητας τους στο εργαστήριο υλικών με ενέπνευσαν να ασχοληθώ με την επιστήμη των υλικών σε προπτυχιακό αλλά και μελλοντικά σε μεταπτυχιακό επίπεδο.

Παράλειψη μου τελειώνοντας αυτό τον κύκλο σπουδών θα ήταν αν δεν ευχαριστούσα τους φίλους μου που με συντρόφευσαν σε όλα αυτά τα χρόνια. Οι πολύωρες συζητήσεις μας, η υποστήριξη στις δύσκολες στιγμές και η πάντα καλοπροαίρετες συμβουλές τους θεωρώ ότι με βελτίωσαν ως άνθρωπο. Οι όμορφες στιγμές που περάσαμε μαζί θα μείνουν ανεξίτηλες και ευχή μου είναι να διατηρηθούν οι σχέσεις μας στον χρόνο.

Το μεγαλύτερο ευχαριστώ όμως το χρωστάω στην οικογένεια μου για την ηθική και οικονομική υποστήριξη σε όποια απόφαση και αν πήρα μέχρι σήμερα, αλλά και για την δημιουργία ιδανικών συνθηκών ώστε να μπορέσω να αφοσιωθώ στην περάτωση των σπουδών μου και στην προσωπική μου εξέλιξη.

Στράτος Κούφης

Abstract

The newly developed 2198 Al-Cu-Li alloy is a promising material for the aeronautical industry due to its unique properties. Li addition reduces density, improves damage tolerance, increases strength and Young's modulus, making the material attractive to several industrial applications. It is thus of high significance to optimise welding performance and simultaneously minimize problems encountered in fusion welding processes. The hot cracking is a limiting factor towards the implementation of the LBW in the industrial applications of the alloy. The current work aims to contribute to the understanding of the mechanism of hot cracking phenomena which develop during laser beam welding (LBW).

A study of the dendrite's morphology adjacent to the crack path has been performed via optical microscopy in order to reveal the microstructure and the crack propagation mode. The grains in the inner region of the weld seem to prefer the equiaxial formation while these on the outer region prefer the columnar formation. Moreover, 0OM showed that the cracks propagate through the grain boundaries. Then, Field Emission Scanning Electron Microscopy (FESEM) equipped with EDX analysis was used in order to evaluate the results from OM and to reveal the chemical composition of the microstructure. The results indicated a structure consisting of equaxial dendrites in the inner region with severe segregation of Cu within the interdendritic region. In order to conduct a further investigation of the segregation phenomena, spot scans were performed in strategically chosen grains via SEM. The spot analysis results showed that the cracked grains have a tendency to be enriched in Cu on their interior in comparison with the non-cracked.

Furthermore, back-diffusion phenomena evolved during solidification have been simulated via the Brody and Flemings model. The model provides quantitative predictions of micro-segregation. The results have been correlated with the measurements from the EDX analysis and all together have been used in order to determine the hot cracking susceptibility index proposed by Kou. The results showed that the Cu-enriched grains have a higher tendency for cracking and that the restriction of non-equilibrium phenomena during solidification lead to a lower tendency for cracking.

In addition, the Rosenthal weld model was employed to calculate the produced thermal field for specimens welded with different welding settings. The aim was to specify the mushy zone range for each setting. The results showed that the specimens with the widest mushy zones had a higher tendency for cracking. This observation fully agrees with the open literature.

In conclusion, the mushy zone size index seems to work better than the Kou criterion for the examined specimens. The results allow the correlation between the experimental conditions and the tendency for hot cracking and also contribute to the understanding of hot cracking phenomena and the optimization of the laser process.

Περίληψη

Το νέο κράμα αλουμινίου-χαλκού-λιθίου 2198 είναι ένα πολλά υποσχόμενο υλικό για την αεροναυπηγική βιομηχανία λόγω των ιδιαιτέρων ιδιοτήτων του. Η προσθήκη λιθίου μειώνει την πυκνότητα, αυξάνει την αντοχή σε κόπωση, την μηχανική αντοχή του υλικού, καθώς και το μέτρο ελαστικότητας του καθιστώντας το υλικό ελκυστικό για διάφορες εφαρμογές. Γίνεται έτσι αντιληπτή η σημαντικότητα της βελτιστοποίησης των συνθηκών συγκόλλησής του περιορίζοντας τα γνωστά προβλήματα που εμφανίζονται στις κατεργασίες που περιλαμβάνουν τήξη υλικού. Ένα από τα σημαντικότερα προβλήματα είναι αυτό της θερμής ρηγμάτωσης. Ο σκοπός αυτής της διπλωματικής εργασίας είναι να συνεισφέρει στην κατανόηση του μηχανισμού της θερμής ρηγμάτωσης που εμφανίζεται στις συγκολλήσεις δέσμης λέιζερ.

Για να επιτευχθεί αυτό έγινε μια σειρά εργαστηριακών δοκιμών. Αρχικά, μελετήθηκε η μικροδομή με την χρήση οπτικής μικροσκοπίας για να αποκαλυφθεί η μικροδομή καθώς και ο τρόπος με τον οποίον εξελίχθηκαν τα ρήγματα. Τα αποτελέσματα έδειξαν ότι οι κόκκοι στην εξωτερική περιοχή του μέταλλου συγκόλλησης προτιμούν την κιονοειδή διάταξη ενώ αυτοί που βρίσκονται στο εσωτερικό προτιμούν την ισοαξονική διάταξη. Επιπλέον η οπτική μικροσκοπία έδειξε ότι οι ρηγματώσεις αναπτύχθηκαν πάνω στα όρια των κόκκων. Έπειτα, έγινε χρήση ηλεκτρονικής μικροσκοπίας (Field Emission Scanning Microscopy) σε συνδυασμό με EDS (Energy Dispersive Spectroscopy) αναλύσεις για να επιβεβαιωθούν τα ευρήματα της οπτικής μικροσκοπίας αλλά και για να μελετηθούν φαινόμενα μικροδιαφορισμού. Τα αποτελέσματα έδειξαν ότι η μικροδομή αποτελείτε από ισοαξονικούς δενδρίτες στο εσωτερικό του μετάλλου με έντονα φαινόμενα μικροδιαφορισμού που αφορούν κυρίως τον χαλκό. Για περεταίρω διερεύνηση έγιναν σημειακές EDX αναλύσεις πάνω σε στρατηγικά επιλεγμένους κόκκους ώστε να μελετηθεί το προφίλ της κατανομής του χαλκού σε αυτούς. Τα αποτελέσματα έδειξαν ότι οι κόκκοι που εμφανίζουν ρηγματώσεις στα όρια τους έχουν την τάση να αποκτούν μεγαλύτερη συγκέντρωση σε χαλκό στο εσωτερικό τους σε σχέση με τους υπόλοιπους.

Επιπλέον, προσομοιώσεις για την παραγωγή ποσοτικών εκτιμήσεων του φαινομένου το μικροδιαφορισμού έγιναν μέσω του μοντέλου των Broody και Flemings. Τα αποτελέσματα συγκρίθηκαν με αυτά των σημειακών μετρήσεων και όλα μαζί βοήθησαν στον προσδιορισμό του δείκτη τάσης για ρηγμάτωσης που έχει προταθεί από τον Kou. Τα αποτελέσματα έδειξαν ότι η εμπλουτισμένοι σε χαλκό κόκκοι έχουν μεγαλύτερη τάση για ρηγμάτωση ενώ ο περιορισμός των εκτός ισορροπίας φαινομένων κατά της συγκόλληση μειώνουν επίσης την τάση για ρηγμάτωση.

Επιπροσθέτως, το μοντέλο του Rosenthal χρησιμοποιήθηκε για τον προσδιορισμό των θερμικών πεδίων που αναπτύσσονται κατά την συγκόλληση. Ο κύριος στόχος ήταν μέσω του εν λόγω μοντέλου να προσδιοριστεί το εύρος της "Mushy Zone" για διαφορετικές συνθήκες συγκολλήσεων που είχαν πραγματοποιηθεί σε παλιότερη εργασία. Τα αποτελέσματα έδειξαν ότι τα δοκίμια με την μεγαλύτερη "Mushy Zone" είχαν μεγαλύτερη τάση για ρηγμάτωση, κάτι που αναμένεται να ισχύει και σύμφωνα με

την βιβλιογραφία.

Ο δείκτης του εύρους της "Mushy Zone" δούλεψε καλύτερα από το κριτήριο του Kou για τα συγκεκριμένα πειράματα. Συμπερασματικά, τα αποτελέσματα της εν λόγω εργασίας συνεισφέρουν στην συσχέτιση των συνθηκών συγκόλλησης με την τάση για εμφάνιση θερμής ρηγμάτωσης ενώ συνεισφέρουν και στην κατανόηση του φαινομένου της θερμής ρηγμάτωσης κατά τις συγκολλήσεις με δέσμη λέιζερ.

Contents

List of Figures

List of Tables

Chapter 1

Introduction

1.1 Aim and structure of the diploma thesis

The aim of this work is to provide an in-depth understanding of the hot cracking mechanism in laser beam welding of the Al-Cu-Li alloy 2198. In order to achieve that, it is necessary to have a detailed theoretical definition of the phenomenon. Then, experimental and simulation results are evaluated according to the theory. The results allow the correlation between the experimental conditions and the tendency for hot cracking and thus contribute to the understanding of hot cracking phenomena and the optimization of the laser process.

In chapter one, a brief review of the Al-Cu-Li alloys is presented, along with an introduction to laser beam welding and to the hot cracking phenomenon.

In chapter two, the aluminum alloy 2198 is presented and also some useful simulation models from the literature are reviewed.

In chapter three, the experimental work is presented. Optical and scanning electron microscopy revealed the as-welded microstructure and Energy Dispersive X-Ray analysis showed information about the chemical composition of the specimens.

In chapter four, calculations have been made using the chapter's two presented simulation models, which have contributed in the explanation of the phenomenon.

In chapter five, the results from the chapters three and four are discussed and comparisons are made wherever relevant.

In chapter six, the conclusions that occur from the study are presented

1.2 Al-Cu-Li Alloys

Around 1919 researchers in Germany studied aluminum alloys containing lithium. The high solubility of lithium in aluminum at high temperatures combined with the low solubility at low temperatures motivated their research since it had already been established that this is the key characteristic for age hardening because of the precipitation occurring from a supersaturated solid solution. The first alloy containing lithium was the alloy "Scleron" with a nominal composition of Al - 12Zn - 3Cu - 0.6Mn - 0.1Li. This alloy showed great resistance to wear, high tensile strength and resistance to corrosion and oxidation. However researchers contested the strengthening effect of lithium additions to aluminum so Scleron production was stopped.

In 1950, metallurgists in Alcoa discovered that lithium increased the elastic modulus of aluminum and they designed the high strength Al-Cu-Li alloy 2020 in 1957 with a nominal composition of Al - 4.5Cu - 1.1Li - 0.5Mn - 0.2Cd. This material showed great resistance in creep and it was used on the United states Navy RA 5 C Vigilante aircraft. No failure was noticed for over 20 years.

Al-Li alloys are attractive for aerospace applications because they have lower density and higher modulus than conventional aluminum aerospace alloys. However the brittleness of 2020 stopped its commercial production.

The second Generation of Aluminum-Lithium Alloys contained around 2% or more Li, around 2% or more Cu, some Mg, and Zr to control grain structure. This generation saw limited applications, mostly in secondary structure on aircrafts. Their biggest disadvantages were the high anisotropy of mechanical properties, crack deviations and delamination problems during the manufacture of parts.

The third Generation of Al-Li alloys was developed in the late 1980s and they contained less than 2% Li. Finally, a number of the new alloys are currently being used, for example: F16 Fighter Aircraft (2297), the A380 Airbus (2196), the Boeing 787 Dreamliner (2099/2199) and A350 Twin-Engine Aircraft (2198)[9].

Figure 1.1: The Airbus A380 (www.airbus.com)

1.3 Laser Beam Welding

The Laser Beam Welding (LBW) method has been employed by several industrial sectors during the recent years. Generally, it is preferred for applications where the exact determination of heat input is a critical factor.

The LBW method is used in the automotive industry, aeronautical industry and defense industry. Moreover, this method has been involved also in the construction of microelectronic components.

The most important factor that makes the LBW method different from the other welding methods is the ability to deliver a high amount of power (order of $10^7 W/cm^2$) to a significantly small area of the material in a very short period of time (order of microseconds).

Furthermore, some of the advantages of the LBW method are the low thermal stresses induced to the workpiece, the limited heat affected zone, the complete control of heat input and the ability to automate of the procedure which gives high rates of productivity[11]. [Fig 1.2] depicts the Laser Beam Welding set up.

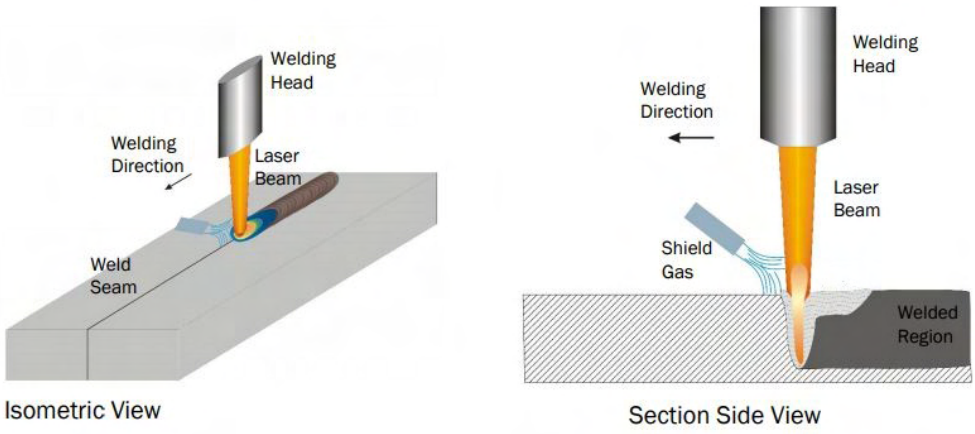

Figure 1.2: Laser Beam Welding set up (www.blog.alfamm.ro)

1.4 Hot Cracking

Hot cracking derived its name from the fact that it occurs in the last stage of solidification where the material's temperature is still high. In the last stage of solidification the formed dendrites are surrounded by a thick film of liquid metal. At the same time, high tensile stresses occur on the weld metal due to the constraints that the base metal applies to the weld metal shrinkage. So, the liquid film cannot transfer the stresses and as a result the grains are separated and they are not able to create a bond. As a consequence, the cracks propagate across the dendrite boundaries. The main factors favor the cracking formation are the wide solidification temperature range, possible impurities in the weld pool, the grain morphology of the weld metal, the tensile stresses and the mechanical constraints that are applied for the stabilization of the welded parts[5].[Fig 1.3] shows a hot crack that follows the welding seam in an aluminum alloy welding.

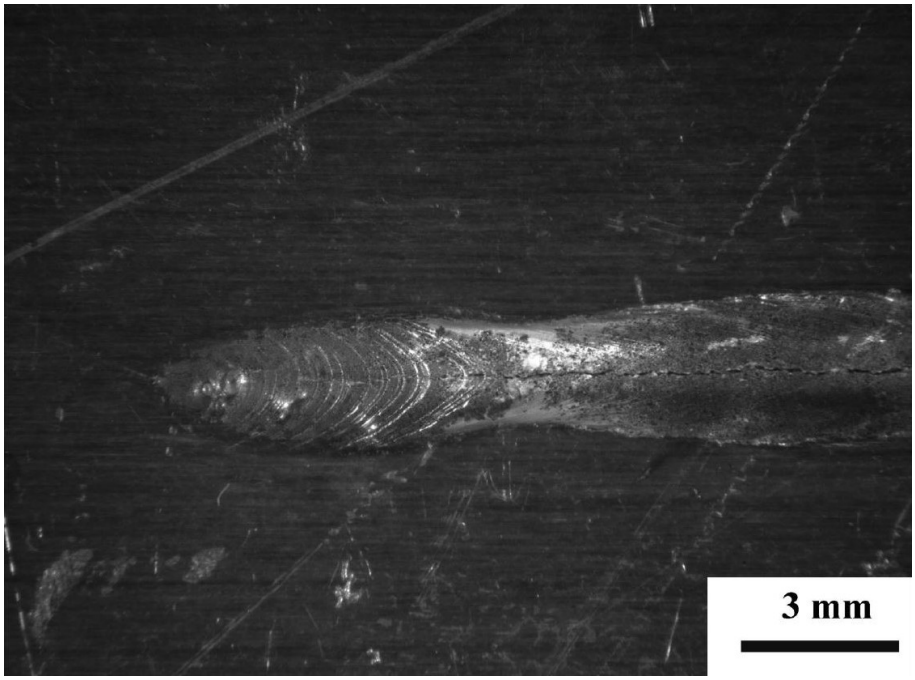

Figure 1.3: Hot cracking in Alumunim alloy welding[11].

1.5 Recent trends

The scientific community puts a lot of effort into understanding the behavior of the newly developed Al-Cu-Li alloy. Among a variety of desired properties that will be discussed later, the lower density due to Li additions makes it differ from the other commercial aluminum alloys. Studies focus a lot on the material behavior under fatigue conditions due to its ability to be used in aeronautical applications. Moreover, the degradation of the mechanical properties due to corrosion phenomena has also aroused the interest. Furthermore, the 2198 alloy can be strengthened by ageing procedure and as a result, research has been made into understanding the precipitation mechanism of the strengthening phases. Due to its potential to be used in lightweight applications it is obvious that there is a need to produce reliable welds with this alloy. In order to achieve that, the advanced methods of Laser beam welding (LBW), Electron beam welding (EBW) and Friction Stir Welding (FSW) are studied in order to be optimized, aiming to produce welds that are reliable for commercial use.

Chapter 2

Literature review

2.1 The 2198 Al-Cu-Li alloy

The newly developed 2198 Al-Cu-Li alloy is a promising material for the aeronautical industry due to its unique properties. The Li addition reduces density, improves damage tolerance, increases strength and Young's modulus making the material attractive to several industrial applications. It is known that each 1 wt.% of Li added to Al reduces density by 3% and thus, increases the elastic module by about 6%. This alloy belongs to the Al-Cu-Li alloys that can be age-hardened. Moreover, the peak strength of these alloys is known to arise from a fine dispersal combination of δ', θ' and T_1 precipitate phases[14]. The chemical composition of the alloy in % wt. is given in the table below [Table 3.1][11].

Table 2.1: 2198 Aluminum alloy chemical composition.

Alloy	Si	Fe	Cu	Mn	Mg	Cr	Zn	Zr	Li	Ag
2198	0.08	0.10	3.50	0.5	0.80	0.05	0.35	0.18	1.10	0.50

In the current thesis, the 2198 alloy has been heat treated to T8 condition (solution treatment, quenching, pre-deformation under tension, and peak aging at $175°C$). The resulting microstructure on three planes (normal direction (ND), transverse direction (TD)) and rolling direction (RD)) is shown in [Fig 2.1]. Using TEM images [Fig 2.2] of BM2198-T8 viewed along $[011]_{Al}$ axis, the diffraction spots from different phases can be identified by the inter-planar distances, crystal structures and orientation relationships with the Al matrix. The identified phases were T1 (Al_2CuLi), $\beta'(Al_3Zr)$ and $\theta'(Al_2Cu)$ [15]

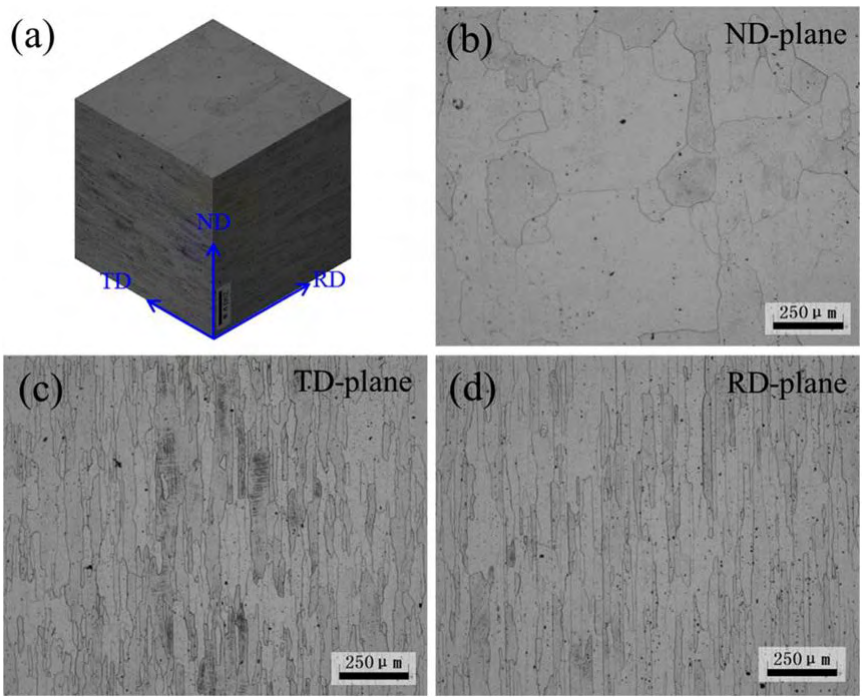

Figure 2.1: Microstructures of 2198-T8 observed using OM on different planes: (a) 3D view of the grain structure; (b) ND; (c) TD; (d) RD [14]

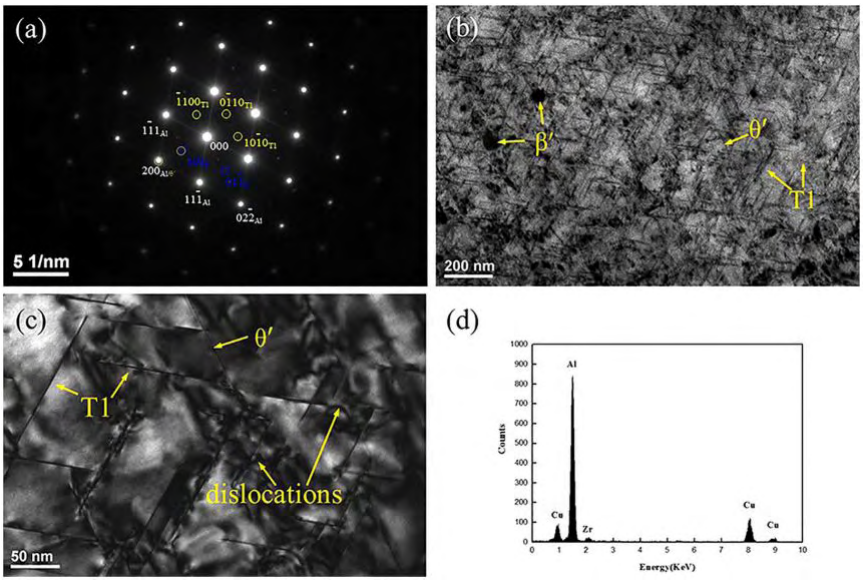

Figure 2.2: TEM images of BM2198-T8 viewed along $[011]_{Al}$ axis: (a) SAED patterns; (b) BF image; (c) magnification of Fig. 3b showing dislocations; (d) EDS analysis of β' (Al_3Zr) phase.[14]

Taking into account all the above, it is easy to understand the significance of the weldability study of this alloy because of the further weight reduction that would occur in plenty of applications such as the aeronautical industry. The research efforts for the Al-Cu-Li alloys focus on four different aspects: (i) porosity formation and control, (ii) weld cracking susceptibility(Hot cracking), (iii) mechanical property characterization and optimization, and (iv) resistance to corrosion.

Weld metal porosity is a common defect in fusion welding processes. We can separate the porosity formation into two categories, the interdendritic porosity which occurs when gas bubbles are trapped between dendrite arms during solidification and the bulk porosity which occurs due to the supersaturation of gases in the weld pool. It is believed that oxides of Li, Mg and Al form at elevated temperatures during heat treatments or hot working and result in a higher tendency for porosity formation. This statement is confirmed by the fact that oxide skin removal before the welding leads to a significantly reduced porosity.

Aluminum alloys such as the 2198 show a significant tendency for hot cracking due to their large solidification temperature range, the existence of low-melting constituents, the high coefficient of thermal expansion and high shrinkage stresses. Cracking occurs near the end of the solidification where the solid-solid interface has low coherence and as a result is not able to withstand the stresses. It has been recommended that filler metal from aluminum alloy 4047 be used in 2198 welding in order to reduce the tendency for cracking[9].

Even without the above defects, the Heat Affected Zone has less strength than the base metal. This reduction is associated with the dissolution and coarsening of hardening precipitates and the softening of cold-worked material. [Fig 2.3] shows the microhardness profile that has been measured with Vickers hardness test on 2198 aluminum alloy (200g 10 seconds)[11].

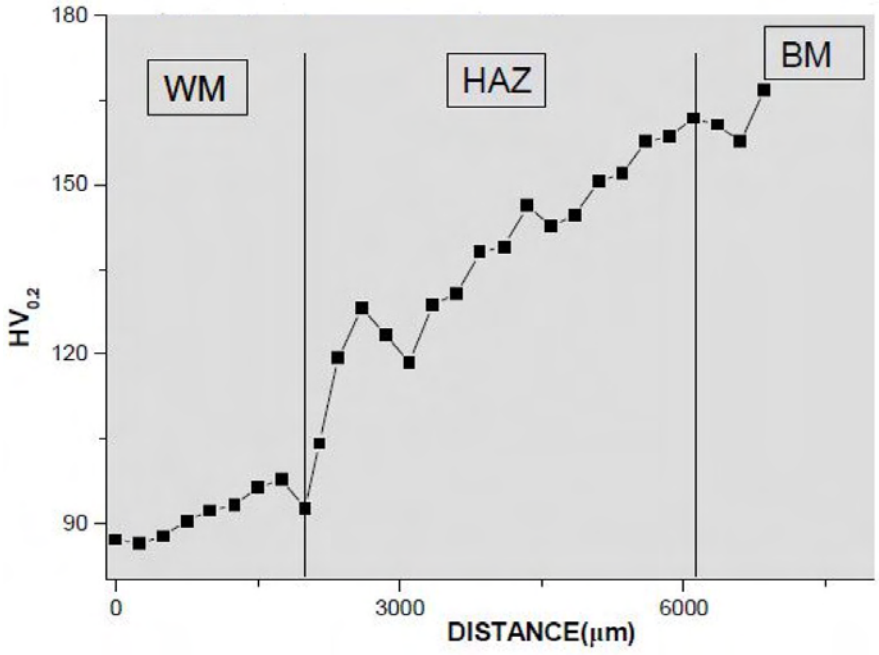

Figure 2.3: Vickers hardness test on 2198 aluminum alloy (200g 10 seconds) [11]

In addition, Al-Li alloys are susceptible to corrosion when exposed to aqueous chloride-containing environments. Furthermore the corrosion properties of the fusion zone are often inferior to those of the base metal. The lower resistance can be connected with the existence of Cu-rich regions at the grain boundaries which is a result of non-equilibrium solidification.

Given the aforementioned problems, a lot of interest is placed in solid-state welding processes where there is no melted metal during the welding such as friction stir welding (FSW)[9].

2.2 Hot Cracking

Examining the phenomenon in a microscopic scale, during welding the region where the temperature is between the solidus and the liquidus is called "mushy zone". This zone forms at the last stage of solidification and it has a high tendency for hot cracking. This is due to the fact that solidification shrinkage is caused by the higher density of the solid than the liquid and thermal contraction occurs while the temperature is falling and as a result, obstructed shrinkage induces tension in the mushy zone. This tension tends to separate the growing grains and consequently a void might form. However, at the same time the grains grow in a lateral direction toward each other to bond together (called bridging), the liquid of melted metal flows between grain boundaries, both phenomena helping the materials to resist cracking. To sum up, the formation of a void occurs when the rate of space increment between two grains due to grain separation is higher than the rate of space reduction due to lateral growth and liquid feeding. This criterion was proposed by Sind Kou in 2015 and it will be discussed later [6][8].

On the other hand, on a macroscopic scale it is easier to correlate hot cracking with the selected welding conditions. According to the literature, there are three main factors that affect the tendency for cracking. The thermal cycle, the solidification range and the restraint intensity[Fig 2.4]. Experiments on Al alloy 2198 showed that correct application of the appropriate pre-loading, pre-heating, focus spot diameter, laser power and welding velocity can reduce the susceptibility for cracking. The greatest reduction was achieved through an approach that has to do with minimalisation of the mushy zone during welding. So, high heat input associated with low laser welding velocity and low laser power, showed low tendency for cracking since these settings result in a small melt pool and as a consequence in a small mushy zone[3].

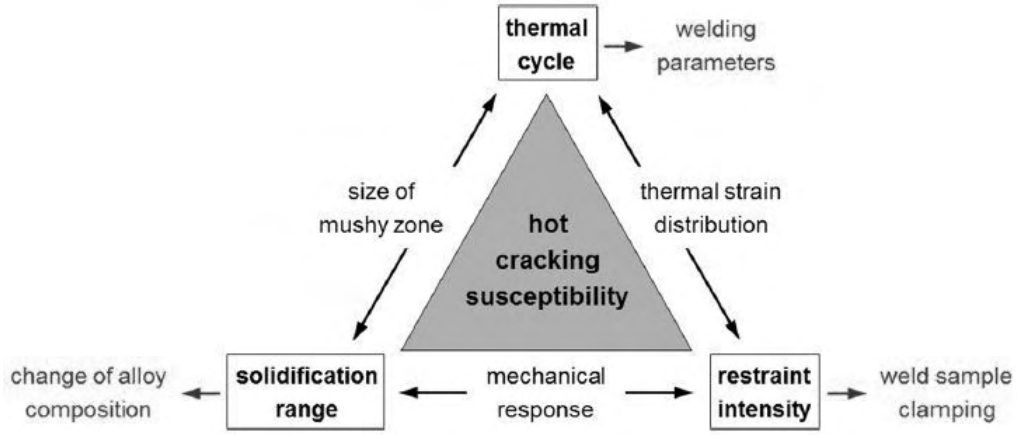

Figure 2.4: Influencing factors on the hot cracking susceptibility[3]

2.3 Segregation phenomena

Segregation phenomena are very common in welding and casting procedures and there are connected with the solidification conditions. During Solidification, the solid-liquid interface compositions can be calculated for each phase via the equilibrium phase diagrams. Given enough time for diffusion (small temperature decrease rate) the calculated compositions can also describe the whole extent of solid and liquid phases, so at the end of the solidification the alloy's composition will be the same in every spot and it will be equal to the nominal one. However during welding, and especially during LBW, the solidification time is too short to achieve homogenization diffusion. At this point it worth to mention that we assume infinitely fast diffusion in the liquid phase. As a result, low or even negligible diffusion leads to significantly low element concentration in the first formed solid, always compared with the equilibrium situation. At the same time the total concetration of alloying elements must remain constant, so the liquid phase is getting enriched in alloying elements as the solidification progresses and this results in remarkably higher concentrations in the latest formed solid. The solidification continues in this way until there is no more liquid to be solidified or the liquid phase composition reaches the eutectic composition where the remaining liquid is solidified through the eutectic reaction. Furthermore the reach of the eutectic point has to do only with the significance of the diffusion. Systems with negligible diffusion conditions will always reach the eutectic point[4].

2.4 Scheil Model

At this point there is the need for a brief review of some common models that describe the solidification of a binary alloy. To begin with, the Scheil model is used when the diffusion in the solid is negligible. Equation (2.1) is known as the Scheil equation.

$$C_s = kC_0[1 - f_s]^{k-1} \tag{2.1}$$

Here, C_s is the solid composition at the solid/liquid interface, k is the equilibrium distribution coefficient, C_0 is the nominal composition of the alloy and f_s is the fraction solid. Equilibrium distribution coefficient k is defined as the ratio of solid to liquid compositions. So, an easy way to estimate k is by dividing the compositions given by solidus and liquidus line equations. Moreover, if both solidus and liquidus lines shape are close to a straight line, like it is in the Al-Cu phase diagram, then we can assume that the coefficient k is constant[2][1].

2.5 Broody-Flemings Model

The Broody Flemings model can be used to estimate the significance of solid-state diffusion during solidification. The solid composition again in the solid/liquid interface, is given by equation (2.2).

$$C_s = kC_0[1 - (1 - 2ak)f_s]^{\frac{k-1}{1-2ak}} \tag{2.2}$$

Here, f_s is a function of temperature given by equation (2.3).

$$f_s = (\frac{1}{1-2ak})[1 - \frac{T_m - T}{T_m - T_l}^{\frac{1-2ak}{k-1}}] \tag{2.3}$$

T_m is the melting point of the pure solvent, T_l is the liquidus temperature of the alloy and a is a coefficient that indicates the significance of the solid-state diffusion. Furthermore, the bigger the a is, the greater the existing diffusion. a is given from the equation (2.4)

$$a = \frac{D_s t_f}{L^2} \tag{2.4}$$

Here, D_s is the diffusivity of solute in the solid (the diffusivity of Cu in Al is $D = 0.000048exp(-16069/T)$[12]), t_f is the local solidification time and L is half the dendrite arm spacing. For aluminum alloys L is given from [Fig 2.7].

Clyne and Kurz have proposed a modification to the B-F model by replacing the a with a', where

$$a' = a[1 - exp(-\frac{1}{a})] - \frac{1}{2}exp(-\frac{1}{2a}) \tag{2.5}$$

This modification reduces B-F model to the Scheil equation when $a \to 0$ end to the equilibrium lever rule when $a \to \infty$[2].

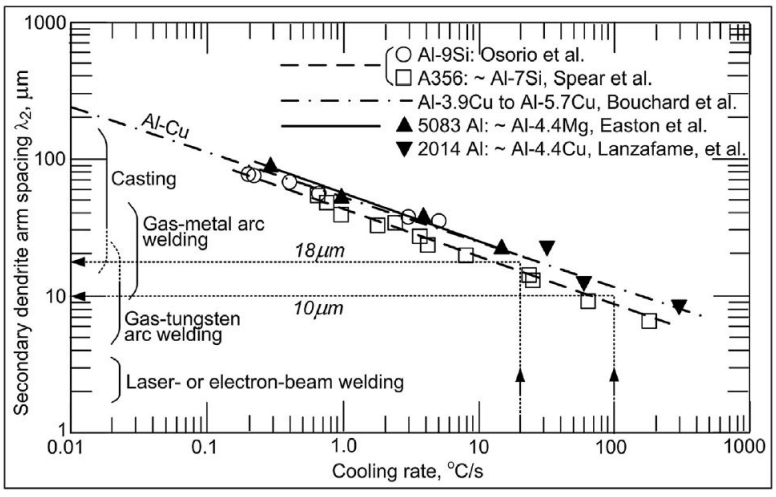

Figure 2.5: Secondary dendrite arm spacing of aluminum alloys with cooling rate [8]

2.6 A criterion for cracking

In 2015 Sindo Kou proposed a criterion for cracking during solidification[6]. In order to do that, Kou chose a control volume Ω which is the space, not the liquid, between two neighboring columnar dendritic grains [Fig 2.6]. Then, he assumed that the left grain is stationary while the right one moves under tension in the lateral direction at the local speed of V_{local}. At the same time, both grains tend to grow at the lateral direction toward each other to bond together (bridging). Moreover, the intergranual liquid flows in the z-direction to feed the grain boundary. It is worth noting that the liquid between the grains is in the form of a thin film at the last stages of solidification. As a consequence, a crack can form in Ω if the rate of net space increase in Ω exceeds the rate of net volumetric flow into Ω. All the above can be described in a quantitative form via the equation (2.6)

$$\{\frac{d\epsilon_{local}}{dT} > \sqrt{1-\beta}\frac{d\sqrt{f_s}}{dT} + \frac{1}{dT/dt}[(1-\sqrt{1-\beta}\sqrt{f_s})u_z]\}_{\sqrt{f_s}\to 1} \tag{2.6}$$

Where ϵ_{local} is the local strain, T is the temperature, t is the time, and $\beta = \frac{(u_L - u_S)}{u_L}$ where u denotes the volume of solid or liquid. Furthermore, the first term of the left hand side describes the grain separation, the first term of the right hand side describes the lateral growth of grains and the second term in the right hand side represents the liquid feeding in the grain boundaries. It is interesting to note that similar equations can be delivered for equiaxed grains. Assuming that they have a spherical shape, $\sqrt{f_s}$ needs to be changed to $\sqrt[3]{f_s}$ and $\sqrt{1-\beta}$ needs to be changed to $\sqrt[3]{1-\beta}$.

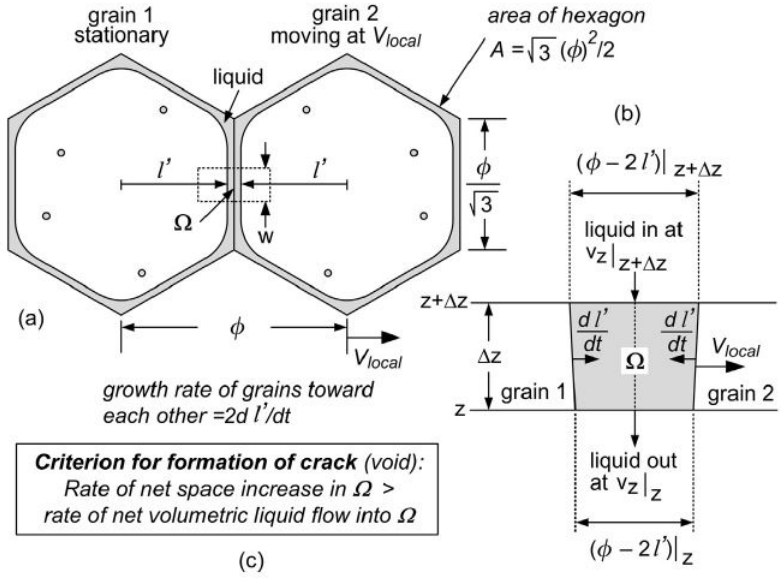

Figure 2.6: Differential control volume X at grain boundary: (a) X located inside dotted box and between two grains (transverse cross-section); (b) X enlarged (longitudinal cross-section); (c) criterion for crack formation in X with preexisting crack initiation sites[6].

Deacreasing $|\frac{d\sqrt{f_s}}{dT}|$ (since $\frac{d\sqrt{f_s}}{dT} < 0$) makes the right hand side of equation (2.6) smaller and hence easier to exceed to cause cracking. As a result Kou proposed the term $|\frac{dT}{d\sqrt{f_s}}|$ as an index for crack susceptibility. A more practical explanation for the significance of the above term is the following. The higher the $|\frac{dT}{d\sqrt{f_s}}|$ is, the smaller the lateral growth rate is, delaying the bridging of the grains. Thus, a higher $|\frac{dT}{d\sqrt{f_s}}|$ results in a longer channel for feeding, making difficult for the liquid to move through it due to the resistance to flow caused by the viscosity of the liquid [Fig 2.7]. As a result, both phenomena lead to higher tendency for hot cracking.

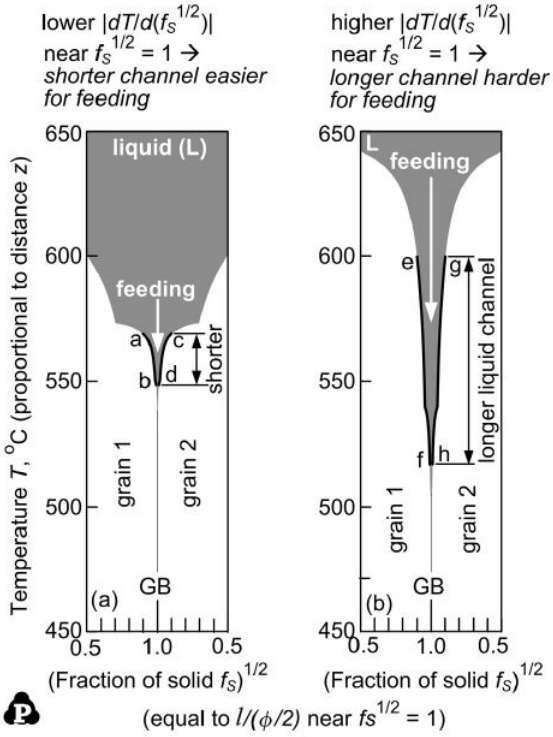

Figure 2.7: Effect of $|\frac{dT}{d\sqrt{f_s}}|$ near $\sqrt{f_s} = 1$ on liquid feeding[6].

2.7 Rosenthal model

The Rosenthal weld model can offer a easy way to estimate the solidification times and the mushy zones size. To begin with, this model assumes a semi-infinite material with its thickness being relatively high compared with the weld dimensions. Moreover, it simulates the heat source as a specific moving point. Furthermore, it assumes negligible heat transfer from the upper side of the material also, the material's temperature remains constant away from the heat source end it is equal with the initial temperature of the metal. The temperature in three dimensions is given from [Equations 2.7-2.9].

$$T(w,y,z) = \frac{Q}{2\pi K} e^{-\frac{u}{2\alpha}w} * \frac{e^{-\frac{u}{2\alpha}R}}{R} + T_0 \tag{2.7}$$

$$R = \sqrt{w^2 + y^2 + z^2} \tag{2.8}$$

$$w = x - ut \tag{2.9}$$

Where, u is the welding velocity, T_0 the initial temperature of the material, α is the thermal diffusivity, Q the heat input and k is the thermal conductivity of the material[5].

Chapter 3

Experimental work

3.1 Experimental Procedure

Specimens have been taken from nine Laser Beam Welds that were prepared for a previous study. All the welds were autogenous and "bead-on-plate" type welds of the aluminum alloy 2198. Also, a mix of 50% Ar (17.5 L/mm) and 50% He (17.5 L/mm) has been used as a protective gas. The welding conditions are provided in [Table 3.1].

Table 3.1: Welding conditions of the examined specimens

Specimen	Power (W)	Velocity (m/min)	Heat Input (J/mm)
1	3441	2	103
2	2970	2	89
3	3913	2	117
4	3252	2	98
5	3441	2	103
6	3630	2	109
10	3441	2	103
11	3252	1.8	108
12	3252	1.6	122

To investigate the mechanism of hot cracking, a series of laboratory examinations were performed. The examinations included stereoscopic examination and optical microscopy in order to study the weld metal microstructure. In addition, scanning electron microscopy (SEM) and field emission scanning electron microscopy (FESEM) were employed for a further microstructure study, both combined with energy dispersive X-Ray analysis (EDX).

The metallographic specimens were prepared using SiC papers (120, 220, 320, 500, 800, 1000 and 2000 grit) and then they were polished using 3μm and 1μm diamond paste. Subsequently, slurry 0.3μm was used in the polishing procedure in order to obtain an even better surface quality. Keller's reagent (2 mL HF 3 mL HCl 5 mL HNO3 and 190 mL water) was used as etchant .

Specimen 10 was selected for a more detailed study due to the existence of a large crack in the middle of the weld metal which is visible to the naked eye. The prepared surface examined using a stereoscope in order to study the morphology of the weld metal and to obtain a more detailed view of the defects such as pores and microcracks.

Furthermore, optical microscopy was employed to characterize the dendrites structure (columnar or equaxial), to identify phases and to determine the crack propagation mode (intergranural or transgranural). In fact, all the above specimens were inspected for cracks via optical microscopy.

Moreover, SEM and FESEM were used for a more detailed observation of the microstructure in order to evaluate the findings from the optical microscopy for specimen 10. The accelerating voltage of 15-20 KV was selected for this purpose.

In addition, EDX analysis was performed in order to extract elemental maps, to estimate microsegregation phenomena and to calculate the chemical compositions of the different phases.

3.2 Stereoscopy

To begin with, the photo below [Fig 3.1] from stereoscope illustrates the macroscopic structure of specimen 10. A large crack is visible in the center of the welding extending from the face to the root of the weld. Moreover, a pore also exists and it is intersected with the crack in the center of the welding. Furthermore it is worth noting that we have a full penetration welding.

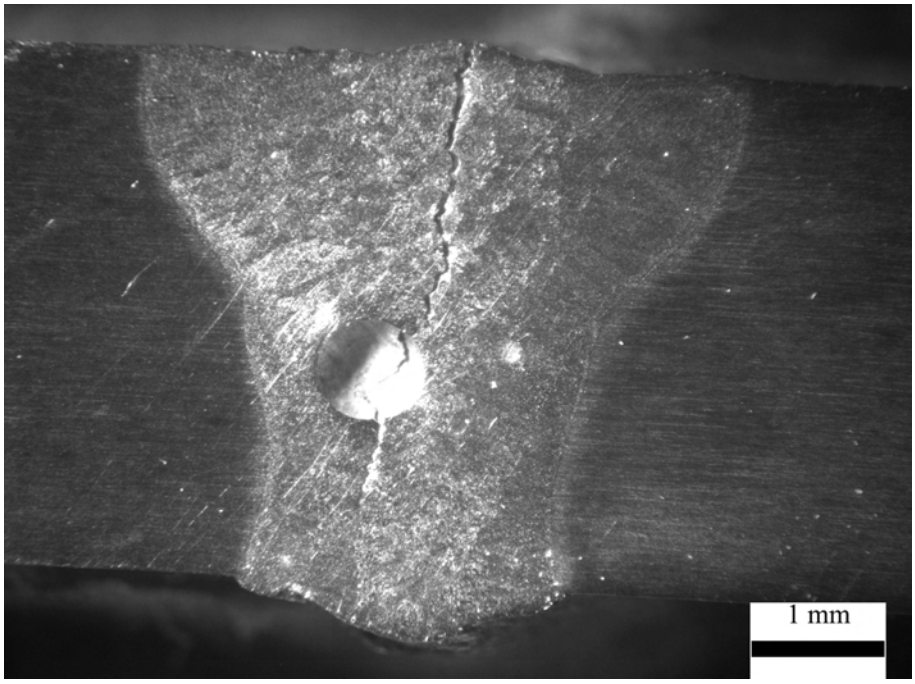

Figure 3.1: Macrostructure of specimen 10 (3441W, 2 m/min)

3.3 Optical Microscopy

Photos taken with different magnification via optical microscopy revealed the microstructure. [Fig 3.4] shows that the alloy has the dendritic microstructure expexted in welding. Furthermore, this photo is divided into two parts. In the left part, which is from the outer region of the weld metal, the grains seem to prefer a columnar structure, while in the right part, which depicts the inner region of the weld metal, the grains exhibit an equaxial structure.

In a higher magnification, some secondary cracks are visible in the weld metal [Fig 3.3]. The crack path of these cracks propagates through the grain boundaries so, the cracking mode is intergranural.

It is also interesting to notice the existence of some particles of a second darker phase that nucleates on the grain boundaries and in some dendrites. This phase seems to have solidified by the end of the solidification.

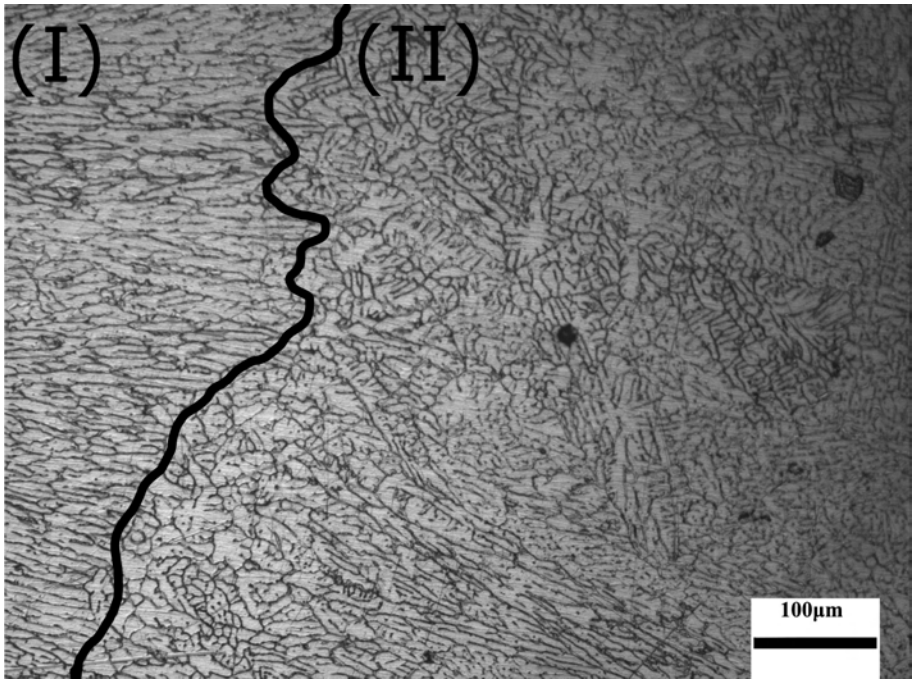

Figure 3.2: Optical microscopy photo from specimen 10: Columnar dendritic grains (I), equaxial grains (II).

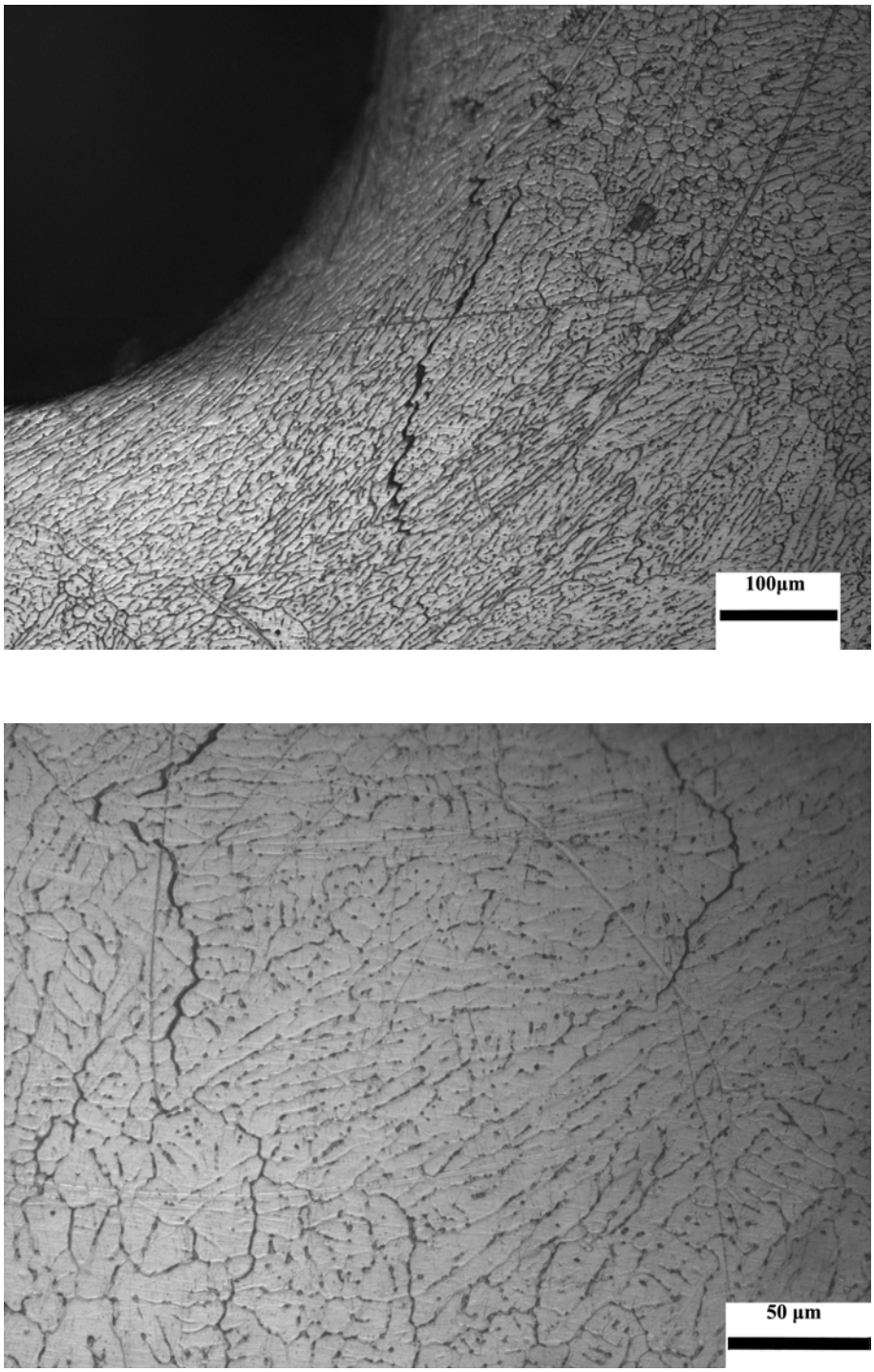

Figure 3.3: Cracks in the weld metal

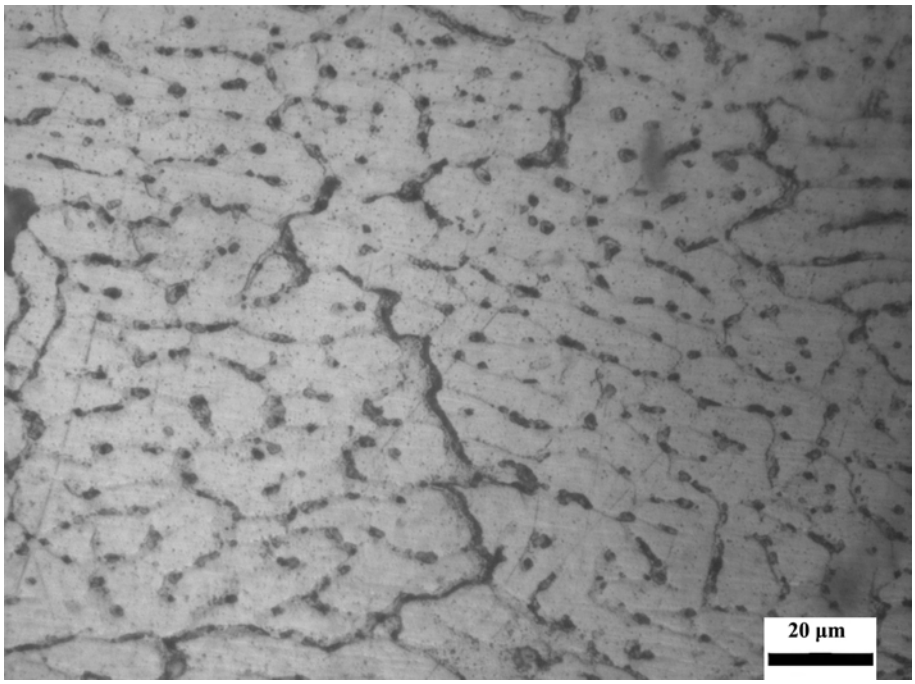

Figure 3.4: Second phase particles between grain boundaries and on dendrites

In addition, all the specimens showed similar results with the same transition from the columnar to equaxial form as we move towards the center of the weld metal. Also the darkest phase on grain boundaries appeared again on the other specimens. Cracks were detected only in specimens 3,6,10 and 12. As it mentioned before, it is believed that there is a strong connection between the crack formation and the size of the mushy zone. In general, a higher heat input leads to a great mushy zone. [Fig 3.5] shows that the higher the heat input the higher is the tendency for cracking.

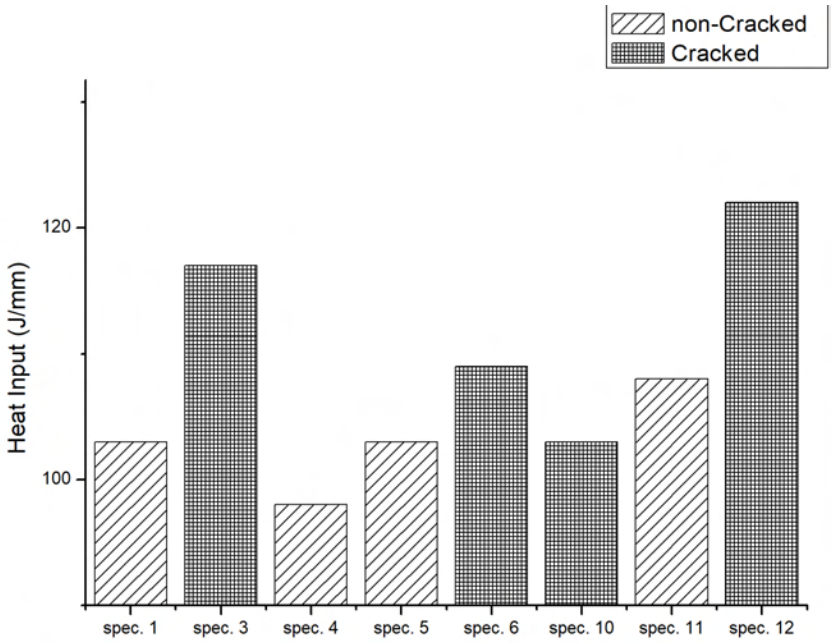

Figure 3.5: Tendecy for cracking formation in correlation with the heat input

3.4 Field emission scanning electron microscopy/ Energy dispersive X-Ray analysis

Field emission scanning electron microscopy was performed to study the specimen microstructure and the crack path. In [Fig 3.6] the brighter phase, which nucleates mainly on the grain boundaries, it is visible again. Also some smaller cracks are visible in the grain boundaries. That fact confirms the intergranural cracking propagation mode stated earlier.

At this point it is interesting to refer to some photos that have been taken from the same welding (welding 10) but at this time a new specimen has been obtained by separating and old one into two pieces (using the main crack as a guideline for the separation) by applying mechanical forces to it. Since the main crack goes from the one edge to the other, it was not difficult to separate the specimen into two parts. Now, looking from a vertical direction, as opposed to the previous view, helps facilitate a further study of the crack morphology. Furthermore in order not to change the existing morphology, the specimen had not had any type of preparation such as polishing or etching. [Fig 3.7] shows the three-dimensional morphology of the dendrites. It is easy to notice that some dendritic grains have separated and as a consequence some secondary cracks propagate again through the grain boundaries.

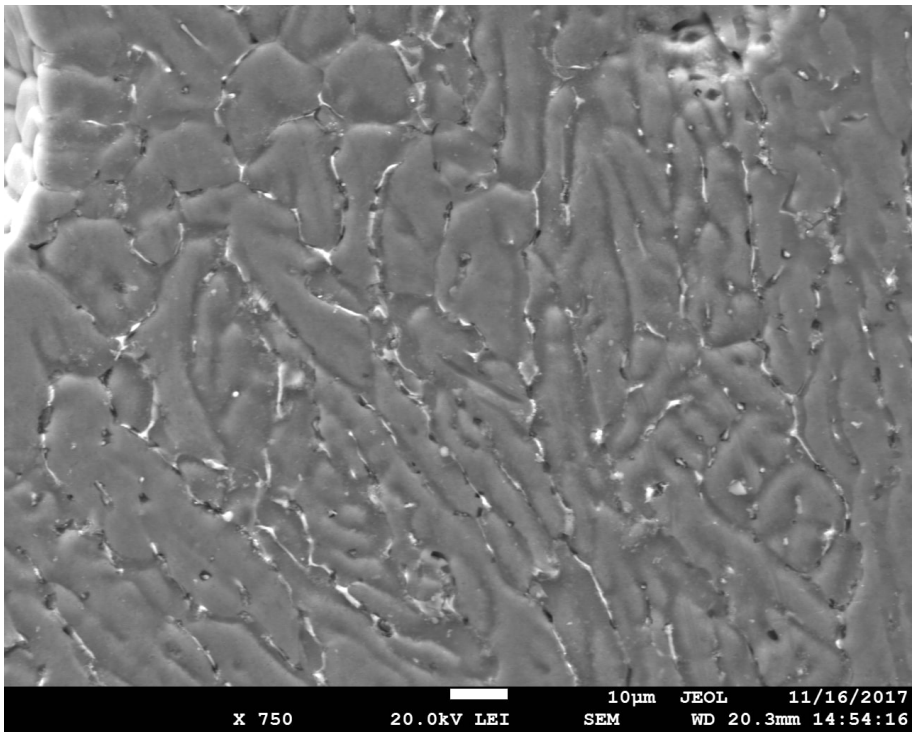

Figure 3.6: Second phase particles between grain boundaries and microcracks

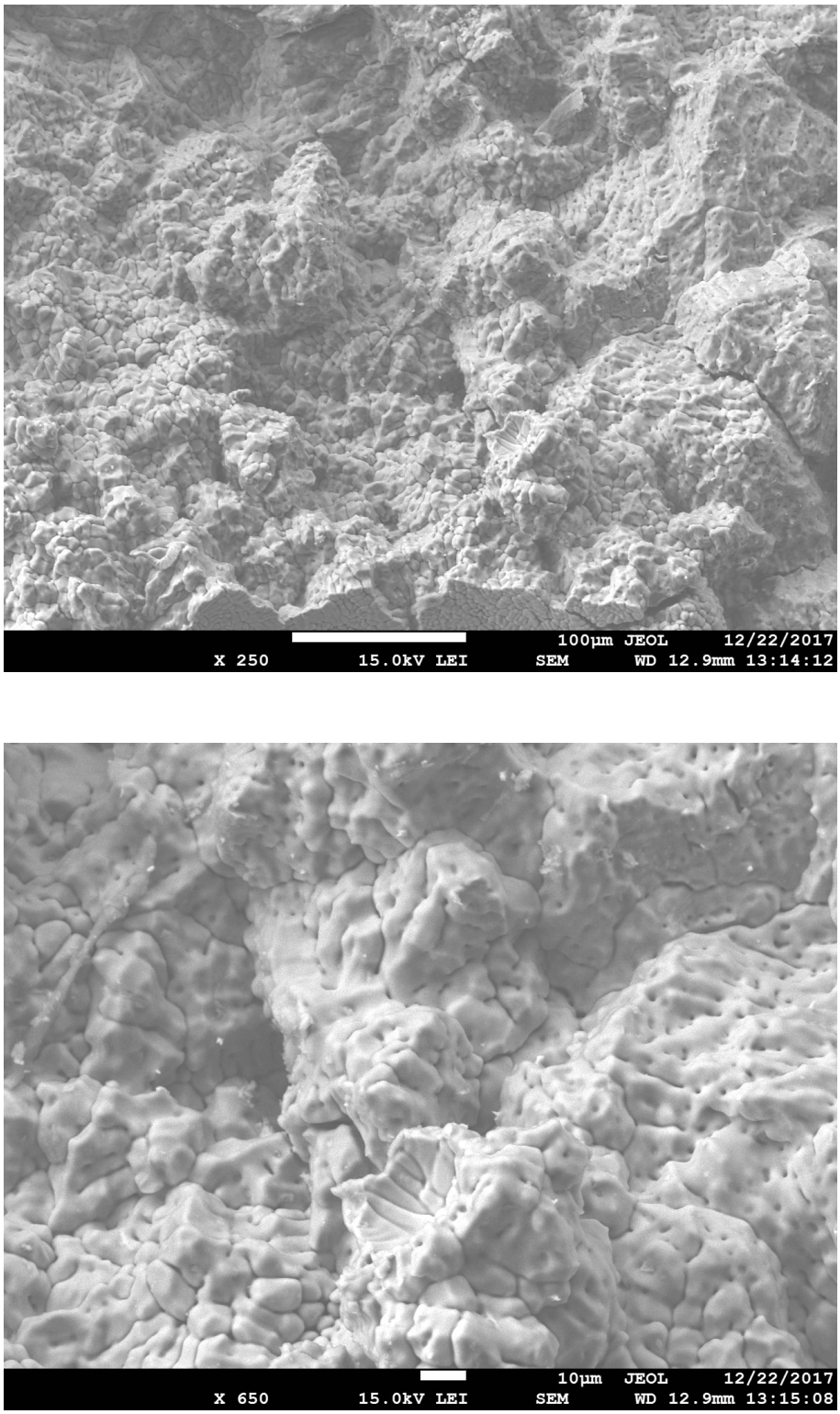

Figure 3.7: Transverse view of the main crack

In order to investigate the redistribution of the alloying elements after solidification, EDX analyses were performed in the polished and etched specimen. The elements mapping showed that the brightest phase is a Cu-rich phase while the darkest phase is an Al-rich phase. The remaining alloying elements did not show any tendency to build up in a preferred region of the microstructure. [Fig 3.8, 3.9]

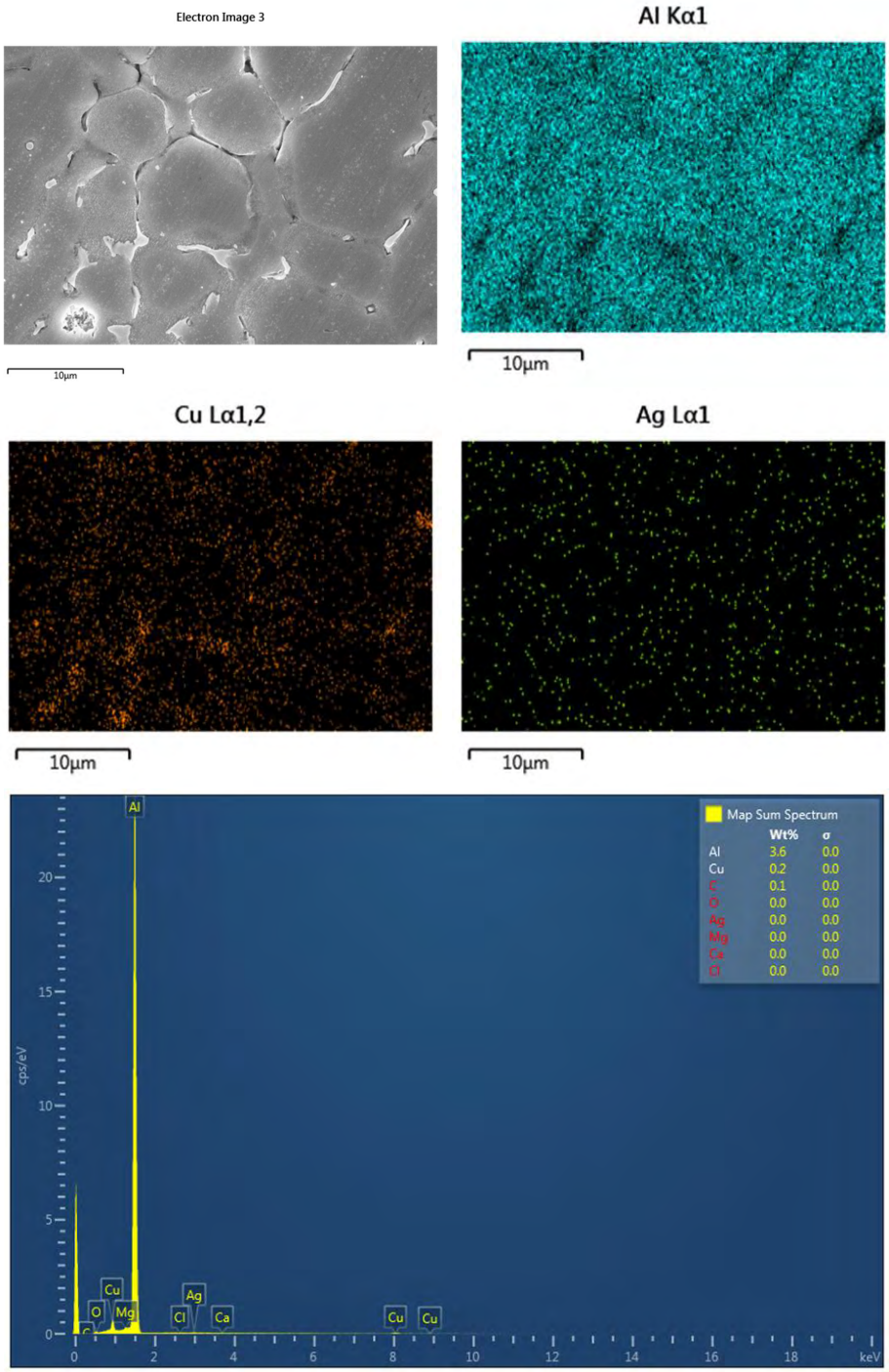

Figure 3.8: SEM image and elements mappings of Al, Cu and Ag in as-welded alloy

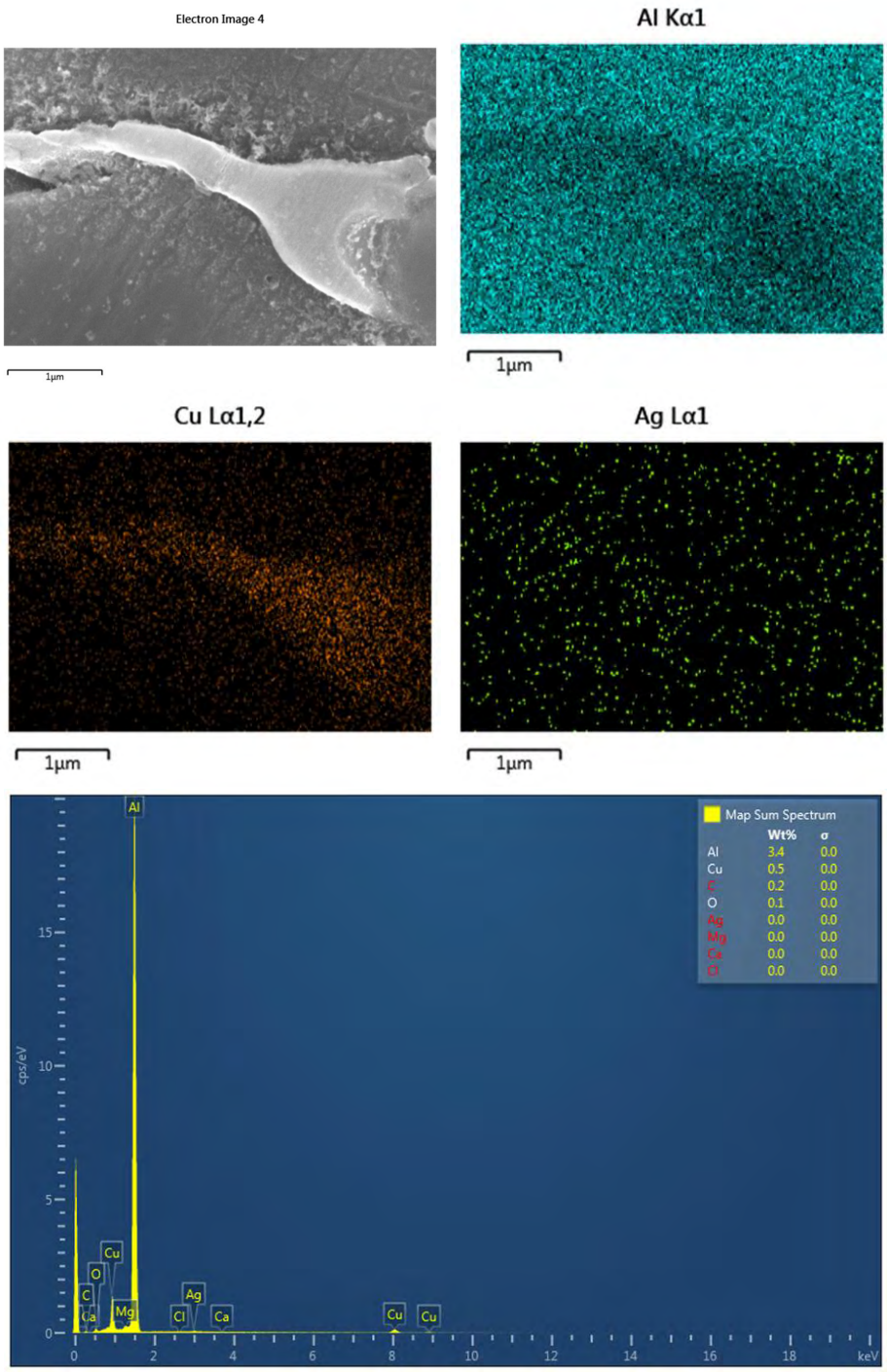

Figure 3.9: SEM image and elements mapping of Al, Cu and Ag in as-welded alloy

3.5 Scanning electron microscopy / Energy dispersive X-Ray analysis

Scanning electron microscopy combined with EDS analysis was carried out in specimen 10. The aim was to analyze cracked and non-cracked dendritic grains in the inner and the outer region of the weld pool. In addition, line and spot scans were produced by EDS analysis for the selected grains. The expected outcome was used to calculate the elemental distribution profile in the dendrites in order to allow comparisons between the cracked and the non-cracked grains. In addition an accurate elemental analysis acquired from the brighter phase located at the grain boundaries was performed.

Line scans provided information about the segregation tendency of the alloying elements.

To begin with, a representative line scan of a non-cracked grain is shown in [Fig 3.10]. It is interesting to notice that the grain is enriched in Cu as we get closer to the outer region while the center of the grain is depleted in Cu. Moreover the increase in Cu concentration occurs against the Al concentration which is lower near to grain boundaries. Considering the other alloying elements segregation phenomena can be also observed but the results showed less significant concentration differences compared with the Cu graphs.

The cracked grains showed the same qualitative behavior with the non-cracked grains with higher Cu concentrations near the grain boundaries [Fig 3.11] so, spot scans were employed for both types of grains in order to obtain quantitative results that can be compared easily.

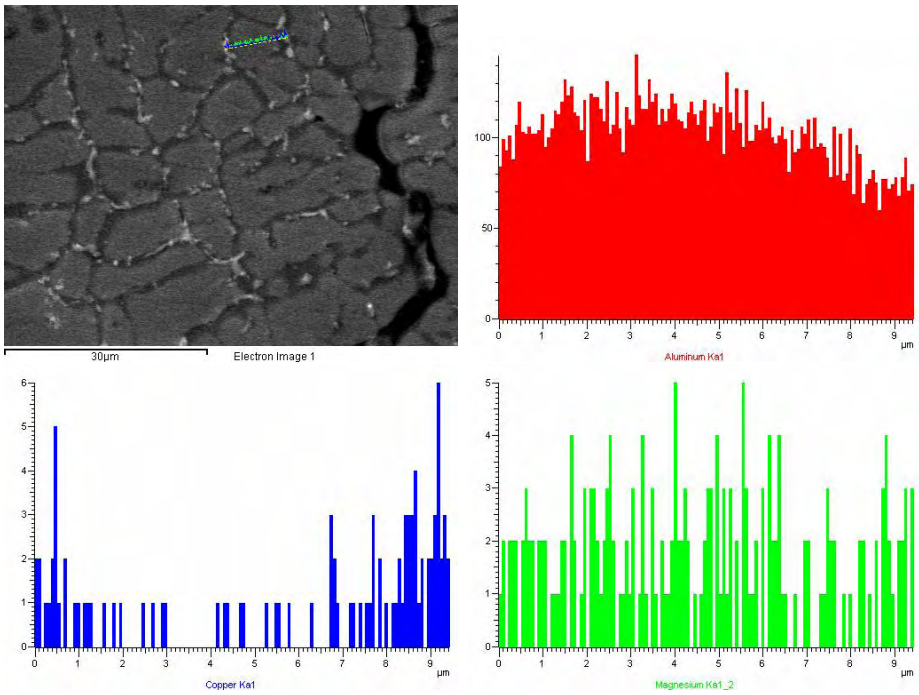

Figure 3.10: Line scan acquired at a non-cracked grain.

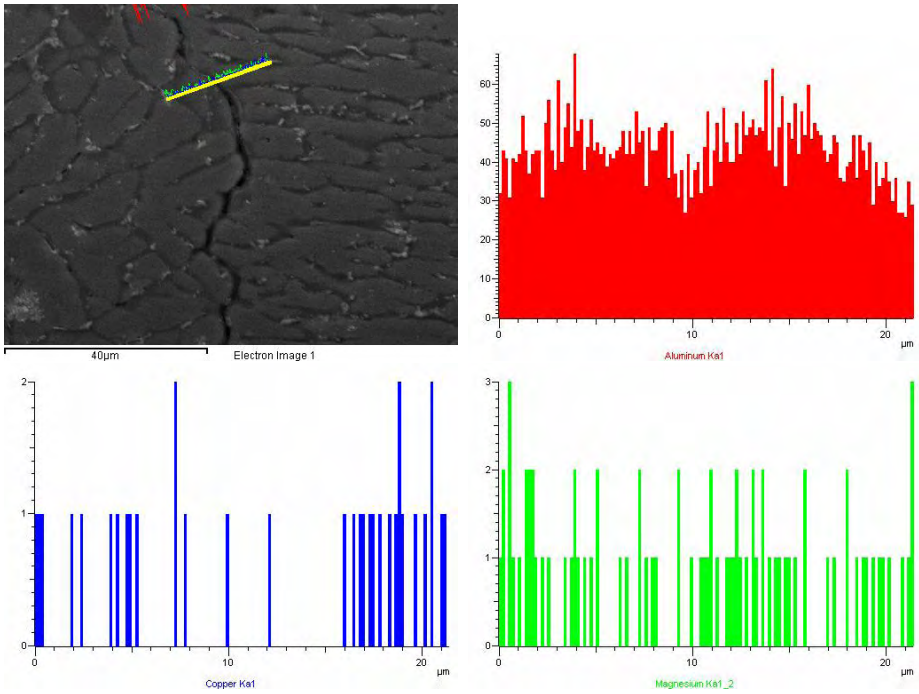

Figure 3.11: Line scan acquired at two neighboring cracked grains.

A significant population of grains were examined. For each grain, cracked or not, 5-9 spot measurements were taken from the one edge to the other, following a "representative" diameter with both the starting and the ending points being on the brighter phase exist at the grain boundaries. The aim was to identify any different trends of elemental distribution between the cracked an the non-cracked grains. [Fig 3.12] and [Fig 3.13] show a representative experiment for a cracked and for a non cracked grain with the results listed in [Table 3.2] and in [Table 3.3] respectively. In order to evaluate all the available results, the examined grains were separated into three groups according to their size and then the results from the analysis were plotted in three different graphs [Fig 3.11]. The results indicated that the cracked grains have a tendency for higher Cu concentration in their interior compared with the non-cracked ones.

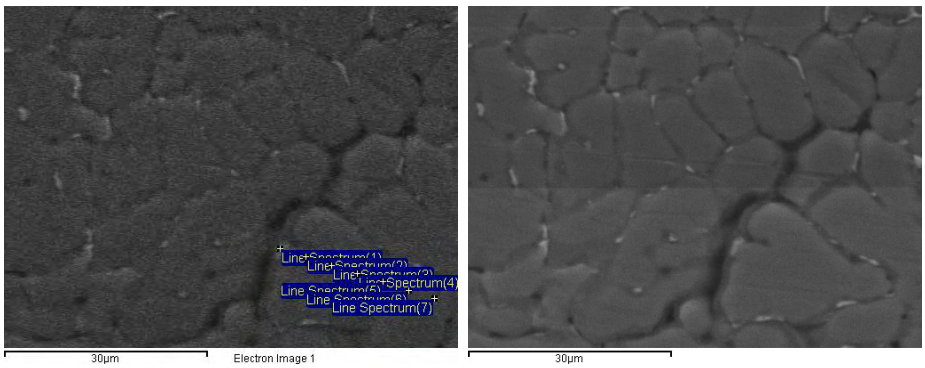

Figure 3.12: Spot scan of cracked grain.

Table 3.2: Spot scan results of a cracked grain

Spectrum	Mg	Al	Cu	Total
Line Spectrum (1)	0	61.91	38.15	100
Line Spectrum (2)	0	100	0	100
Line Spectrum (3)	0	98.46	1.83	100
Line Spectrum (4)	0	96.79	3.20	100
Line Spectrum (5)	0	96.26	3.82	100
Line Spectrum (6)	0.23	96.64	3.14	100
Line Spectrum (7)	0.45	85.28	14.27	100

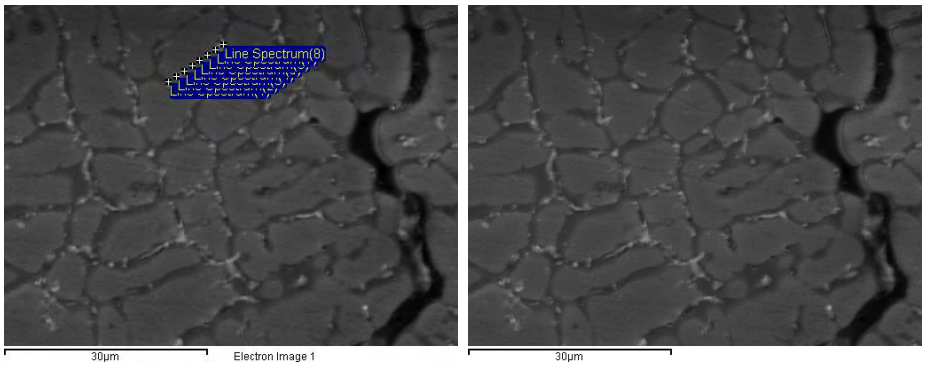

Figure 3.13: Spot scan of non-cracked grain.

Table 3.3: Spot scan results of a cracked grain

Spectrum	Mg	Al	Cu	Total
Line Spectrum (1)	0.76	88.36	10.88	100
Line Spectrum (2)	0.01	99.25	0.74	100
Line Spectrum (3)	0.14	97.91	1.95	100
Line Spectrum (4)	0.05	99.56	0.39	100
Line Spectrum (5)	0.03	99.95	0.02	100
Line Spectrum (6)	0.38	98.76	0.86	100
Line Spectrum (7)	0.37	93.55	6.07	100
Line Spectrum (8)	0	91.76	8.68	100

Measurements were taken from the area where the grains seem to prefer the isocolumnar formation. The results are presented in [Fig 3.14] and [Table 3.4]. The area was crack free and the results showed that the examined area was depleted in Cu compared to the cracked grain in [Fig 3.12].

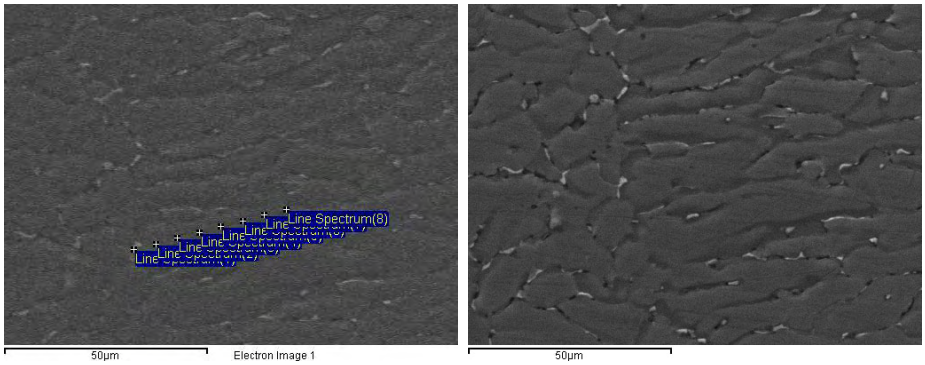

Figure 3.14: Spot scan results of non-cracked grains away from the center of the weld metal.

Table 3.4: Spot scan results of non-cracked grains away from the center of the weld metal.

Spectrum	Mg	Al	Cu	Total
Line Spectrum (1)	0	75.04	25.38	100
Line Spectrum (2)	0.56	97.06	2.38	100
Line Spectrum (3)	0	99.77	0.23	100
Line Spectrum (4)	0.75	97.74	1.51	100
Line Spectrum (5)	0	99.04	1.27	100
Line Spectrum (6)	0	99.24	1.19	100
Line Spectrum (7)	0	97.8	2.66	100
Line Spectrum (8)	0	98.66	1.55	100

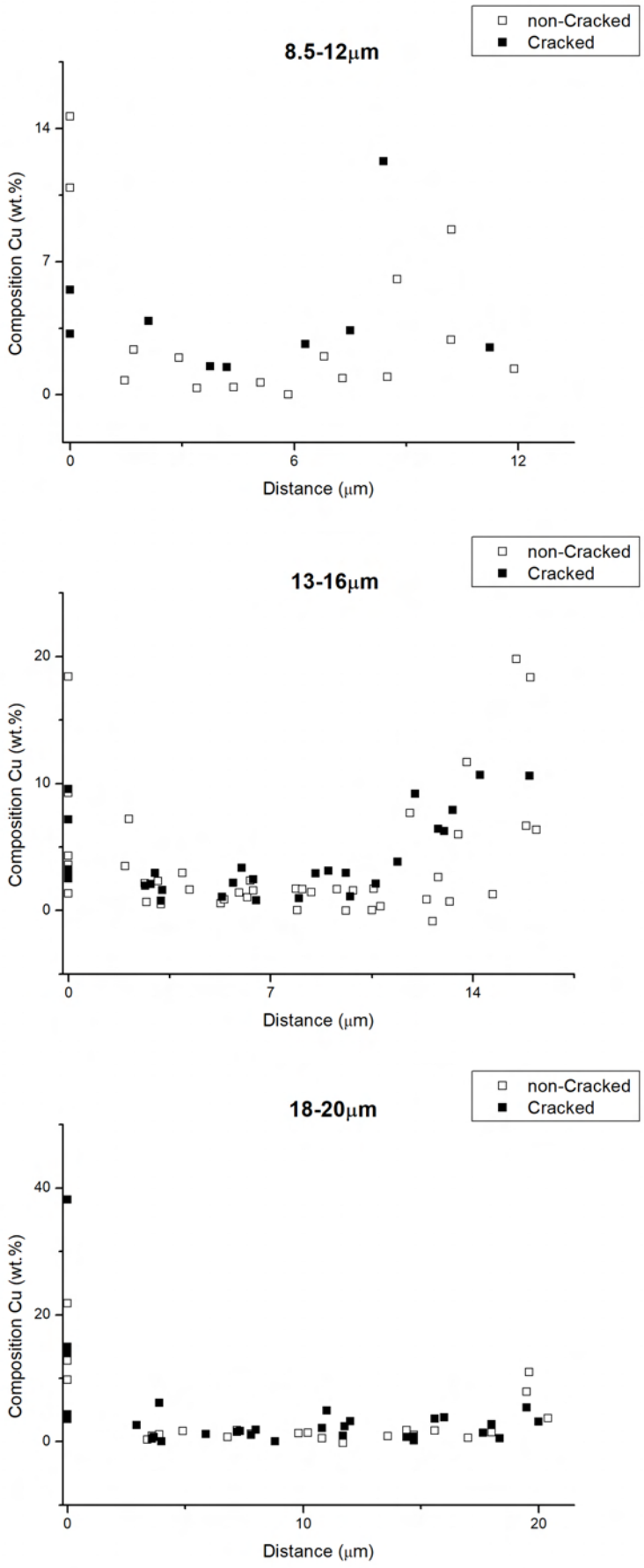

Figure 3.15: Spot scan results of different cracked or non-cracked grains.

An effort has been made to identify the chemical composition of the phase that nucleates mainly on the grain boundaries. For this purpose, spot measurements were taken via the EDX to indentify the composition of the phase [Table 3.5].

The results agreed with those from the elementary maps that were presented earlier and they showed that the examined phase consisted mainly of Al and Cu. Cu consecration measurements vary from 18.63% wt. to 38.15% wt. It is interesting to note that for the case (3) the Cu composition expressed in atomic fraction is 20.73 % At. while the Al composition is 79.27 % At. According to the literature, compositions very close to the one in case (3) have been identified as θ (Al_2Cu) phase [7].

Table 3.5: Spot measures of elementary composition of the second phase particles that nucleate on grain boundaries in %wt.

Spectrum	Mg	Al	Cu	Total
(1)	0	75.04	25.38	100
(2)	0	77.41	22.67	100
(3)	0	61.91	38.15	100
(4)	0.83	76.97	22.21	100
(5)	0	80.79	18.63	100
(6)	0.33	73.85	25.82	100
(7)	0.07	78.12	21.81	100
Average	0.18	74.87	24.95	100

Chapter 4

Simulations

4.1 Scheil and Broody-Flemings Solidification Models results

The experimental results showed that Cu has a significantly higher tendency for segregation, so Scheil & Broody-Flemings Models were employed to describe the solidification and the segregation phenomena of the Al-Cu binary alloy focusing on specimen 10's welding conditions.

The first step was to define the factor α which is given in the equation (2.4). As mentioned in chapter 2, $L \simeq 1.5\mu m$ and $D = 0.000048exp(-16069/T)$ where T is the temperature. Moreover the solidification time for specimen 10 was estimated via the Rosenthal weld model so, $t_f = 0.248Sec$. Furthermore, the above models assume that D is constant but as it is known, diffusion coefficient is in strong correlation with temperature. As a result, a mean value for D was calculated between 648 and $548°C$ where the former is the liquidus temperature and the latter is the eutectic temperature which is the lowest temperature that can occur during solidification. So, the average coefficient diffusion is $D = 7.11 * 10^{-13}$. Using all the above, the calculated value for α coefficient was α=0.314 and with Clyne and Kruz modification [equation 2.5] $\alpha' = 0.199$ (for simplicity we will refer to it as α).

In addition to the calculated value for α, some more values were chosen for comparison (the selected values refer to α' given by Clyne and Kruz modification), calculations were made for α=0, α=0.199, α=0.3 and α=0.5. It is worth noting again that the higher the coefficient the higher the diffusion occurring during solidification.

Lastly, coefficient k had to be estimated. In order to achieve that, solidus and liquidus lines were assumed to be straight lines, so the ratio of solid to liquid composition during solidification can also be assumed constant. The calculated mean value for k, which showed little variation in temperature changes, is $k = 0.172$.

The aim of these calculations was to determine the phases after solidification, to study the resulting Cu concentration grain profile and to produce the $T - f_s$ curve which will be used as an input to the Kou criterion model mentioned before.

The resulting composition in solid-liquids surface and the $T - f_s$ curve during solidification for each occasion is shown in [Fig 4.1] and [Fig 4.2].

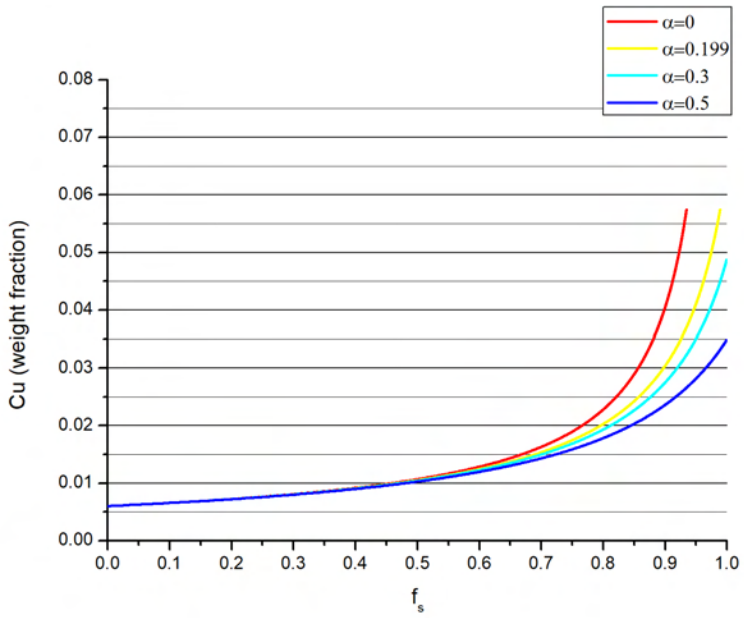

Figure 4.1: Cu composition-Solid fraction diagram produced by Broody-Flemings model.

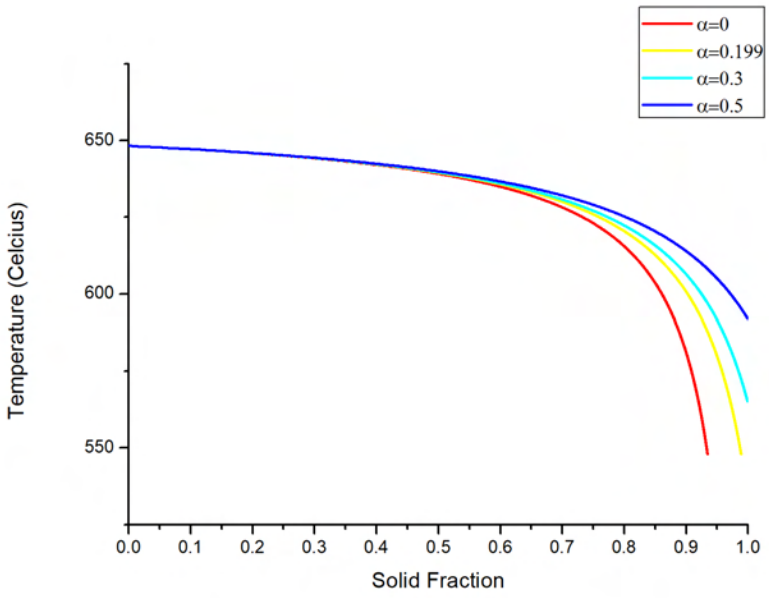

Figure 4.2: Temperature-Solid fraction diagram produced by Broody-Flemings model.

Considering the Composition diagram [Fig 4.1], the lines start to differ after $f_s = 0.5$ with compositions varying from 3.5%wt. (equilibrium) to 5.68%wt (eutectic composition of solid phase). Low α values such as $\alpha = 0$ and $\alpha = 0.199$ lead to the eutectic reaction and as a result the resulting microstructure will consist of a mix of α and θ phases. However, high α values lead the system to avoid the eutectic reaction. For this occasion the microstructure will be consist only of α phase. It is also worth noting that Scheil solidification occurs for $\alpha = 0$ and equilibrium solidification occurs for $\alpha = 0.5$

[Fig 4.3] shows the calculated composition profile of a grain with an approximate diameter of 20μm. For this purpose, in order to convert the solid fraction values to distance on the grain, the dendrites were assumed to be spherical since they prefer the equaxial formation[6].

Equation (4.1) gives the f_s during solidification

$$f_s = \frac{V_{grain}}{V_{grain,final}} \tag{4.1}$$

Where V_{grain} is the volume of the expanding grain during solidification and $V_{grain,final}$ is the grain volume at the end of the solidification. So,

$$f_s = \frac{\frac{4}{3} \cdot \pi \cdot r^3}{\frac{4}{3} \cdot \pi \cdot r_{final}^3} \tag{4.2}$$

$r_{final} = 10\mu m$ so,

$$r = 10 \cdot fs^{1/3} \tag{4.3}$$

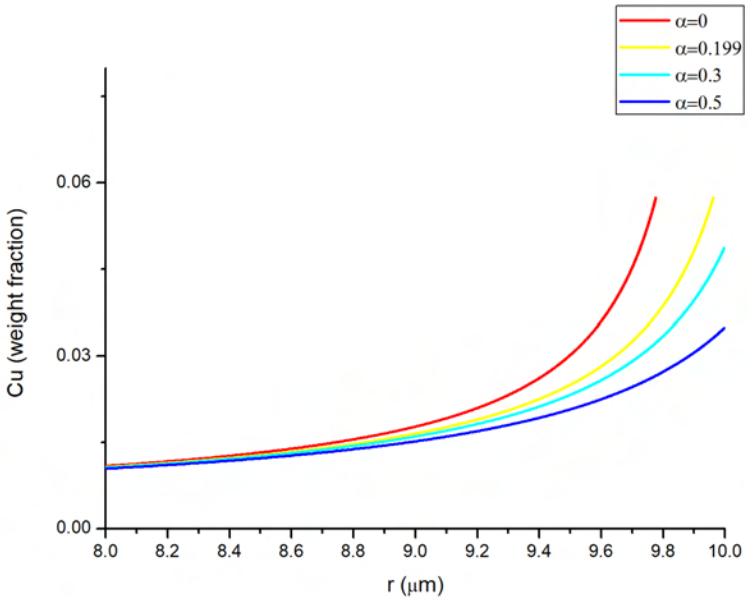

Figure 4.3: Composition of Cu in a representative grain with $10\mu m$ diameter, produced by Broody-Flemings model.

4.2 Hot cracking tendency index

As mentioned before, Sindo Kou proposed $|\frac{dT}{d\sqrt{f_s}}|_{f_s \to 1}$ as an index for hot cracking tendency. In the case of the equaxial grains, such as specimen 10, $\sqrt{f_s}$ needs to be changed to $\sqrt[3]{f_s}$, so the index will be $|\frac{dT}{d\sqrt[3]{f_s}}|_{f_s \to 1}$. The choice of f_s range for the calculations is arbitrary but in general, in low f_s values there is enough liquid for feeding and thus a small tendency for separation, while it is believed that near $f_s = 0.99$ the neighboring grains have growth enough in the lateral direction achieving the "bridging". So, for this occasion, $0.83 < f_s < 0.97$ have been chosen (corresponding to $0.94 < \sqrt[3]{f_s} < 0.99$). Having produced the T-f_s graphs employing the Broody and Flemings model for different values of coefficient α, the index can be calculated by taking the derivative for each occasion. [Fig 4.3] shows the cracking susceptibility index for the different values of α coefficient. It is worth noting that for $\alpha = 0$ the material shows a high tendency for hot cracking but the solidification quickly leads to the eutectic reaction. A lot of liquid remains in the last stage of the procedure which might result in feeding the space between the grains, thereby avoiding the void formation.

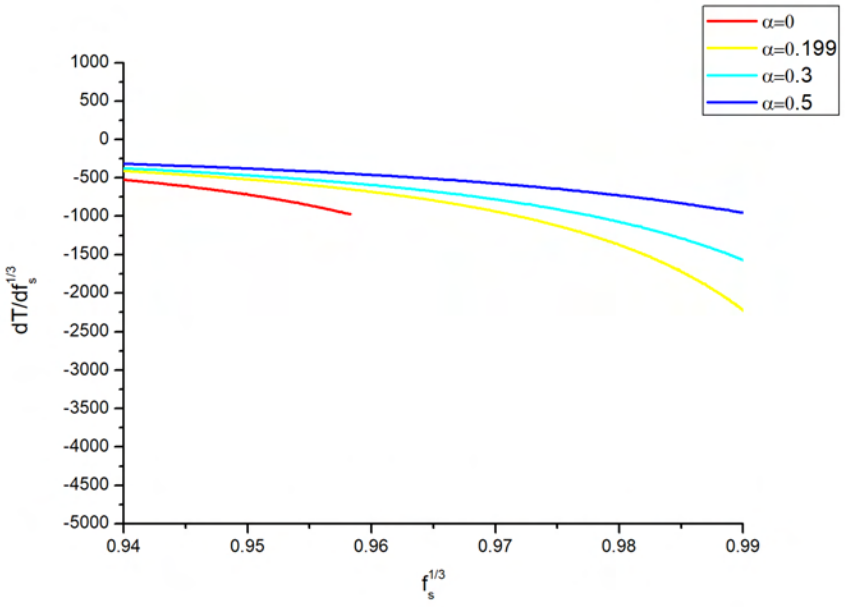

Figure 4.4: Hot cracking susceptibility index for different values of α coefficient.

4.3 Melt pool and mushy zone size calculation via Rosenthal weld model.

The Rosenthal weld model was used to estimate the size of the mushy zone since its significance for the hot cracking formation has been made clear in chapter 2. In order to achieve that, contours were plotted from the top view. The mushy zone is defined as the area where the temperature is between the liquid and the solidus temperature of the alloy so, for this occasion between $648°C$ and $567°C$[13]. Moreover the simulation performed for all the different welding conditions mentioned in [Table 3.1]. [Fig 4.5] shows some representative results for specimens 3 and 4. The white color represents the area where the temperature is above the liquidus temperature , the red area stands for the mushy zone while the gray area is the solid metal. The simulations for all the specimens are summarized in [Fig 4.6]. Generally, the results evaluate that the greater the size of the mushy zone the greater the tendency for cracking.

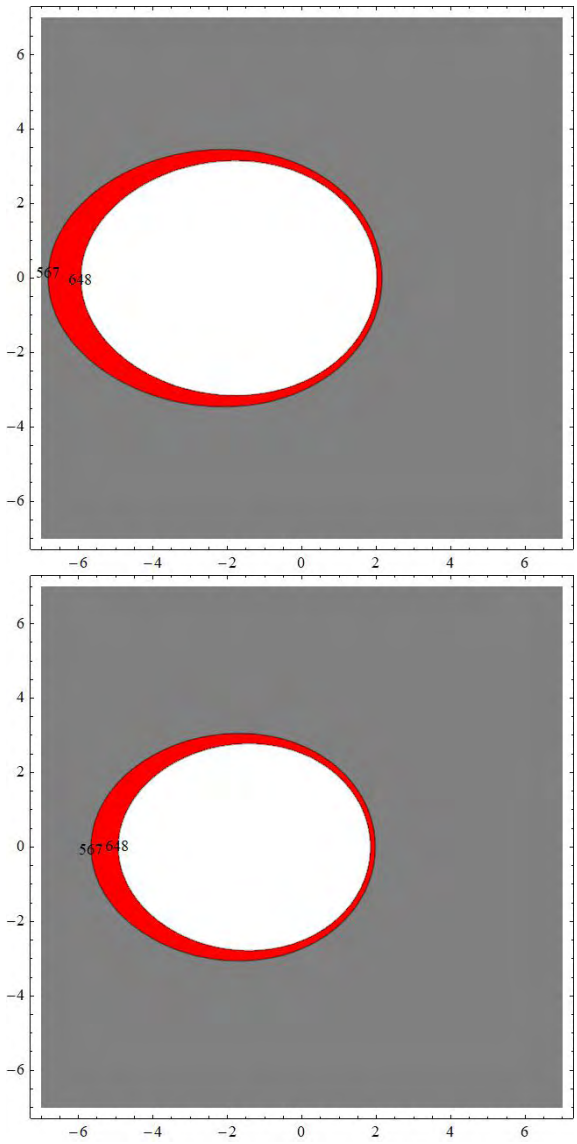

Figure 4.5: Calculated mushy zone and area via Rosenthal weld model.

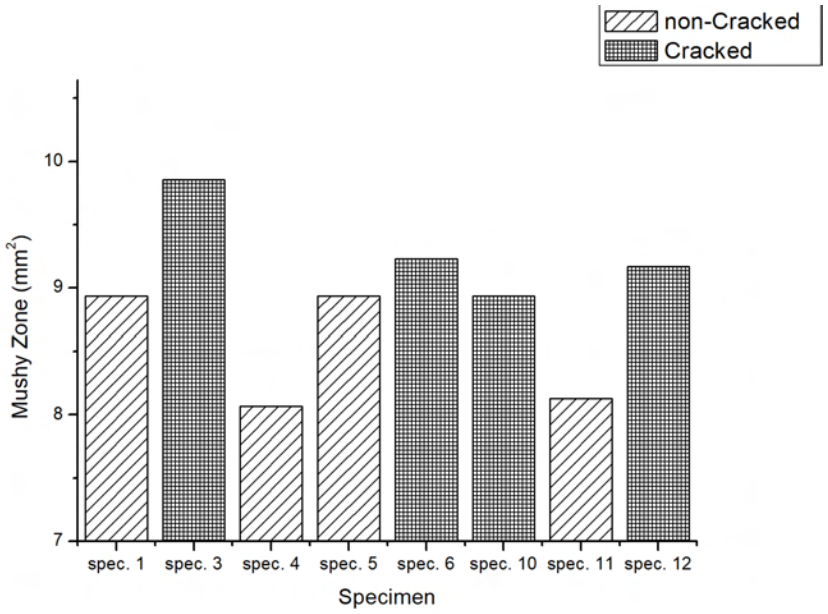

Figure 4.6: Cracking formation in correlation with the mushy zone size.

Chapter 5

Discussion

5.1 Interpretation of EDS analysis results compared with the results from Broody and Flemings model

[Fig 4.3] shows that for every chosen value of α the concentration of Cu ranges from 0.5% wt. to 1% wt. in a range of radius from 0 to $8\mu m$ showing a very slow increase during this range. However, for $r = 8\mu m$ to $r = 10\mu m$ the increase in the concentration is really dramatic and it is strongly connected with α coefficient. The qualitative results from the line scans [Fig 3.10][Fig 3.11] agree with the simulations and show for both occasions that Cu consecration is lower and almost stable in the inner region of the grain while it starts rising rapidly in the outer region.

In contrast, the quantitative results from spot scans do not fully agree with the results from the Broody and Flemings model. For the case of the non-cracked grains [Table 3.3], most of the measurements showed low concentration of Cu in the inner and sometimes also in the outer region of the grain. For the case of the cracked grains [Table 3.2], the concentration of Cu was generally higher than the one of the non-cracked grains in the whole region of the grain and it was higher also than the predicted composition from the broody and Flemings model.

An explanation for the disagreement between spot scan results and the Broody Flemings Model outlined below. It is known that solidification phenomena are dependent on from a variety of factors. Moreover, in the Broody and Flemings model a lot of assumptions were used compared with the real system (binary alloy, constant diffusion coefficient, spherical grains, etc). As a consequence, differences have been observed between the theoretical model and the experimental measurements.

5.2 Kou proposed index

It is obvious from [Fig 3.15] that the cracked grains have the tendency to obtain a higher composition in Cu compared with the non-cracked grains. Furthermore, it is also known that during welding the thermal and the strain field show great discrepancies. The above might result from different local solidification conditions. In the Broody Flemings model the solidification conditions are taken into account by the α coefficient and as mentioned earlier low values of α coefficient lead to higher elementary concentrations close to the end of solidification. So, an explanation for the higher composition of the cracked grains might be the constant lack of diffusion which lead the solidifying grain to obtain an higher and higher Cu composition on its solid-liquid interface.

In [Fig 4.4] it is clear that the lower the coefficient α is, the higher the index (its absolute value) for hot cracking sensitivity proposed by Kou is too. All the above totally agree with the fact that the cracked grains are enriched in Cu compared to the non-cracked grains.

5.3 Mushy zone discussion

In [Fig 3.5] and in [Fig 4.6] a correlation between the mushy zone size, the heat input rate and the formation of hot cracking has been made. It is shown that high heat input and wide mushy zone lead to a high tendency for cracking. Furthermore it is worth mentioning that for the same heat input of $103J/mm$ Specimen 1 and 5 were crack free while specimen 10 showed cracks. At the same time all the specimens with a heat input higher than $103J/mm$ were cracked, except specimen 11 which will be discussed later. All the specimens with a heat input lower than $103J/mm$ were crack free. So, it seems that the heat input of $103J/mm$ works as a boundary between heat input that lead to cracks and heat input that do not lead to crack formation.

Considering the specimen 11, it is interesting to note that despite the high heat input of $108J/mm$ did not lead it to form cracks. Moreover, the resulting area of mushy zone was slightly higher than the mushy zone that have been produced from a significantly lower heat input of $98J/mm$. The explanation for the different behavior of specimen 11 might attributed to the fact that the high heat input rate was achieved with the compination of low power and low speed. As stated earlier in the literature review, in order to minimize the mushy zone and consequently the tendency for hot cracking, a high heat input rate achieved using low power and low speed is the best option.

5.4 Hot cracking sensibility index results vs Mushy zone size index

Generally, in order to achieve low absolute values for the Kou's proposed index, it is also necessary to achieve high values for α coefficient. The most convenient way to control α values is through the solidification time t_f and generally this can be realized by increasing the heat input rate. However, high heat input rates lead to large mushy zones and as a consequence a high tendency for cracking. So, at first sight, these two criteria seem to conflict. Therefore, the ideal situation would be to optimize the welding conditions aiming to have slow solidification times and small mushy zones.

[Table 5.1] shows the solidification times calculated via Rosenthal weld mode and the α coefficient for each specimen while [Table 5.2] shows the calculated area of mushy zone during welding again for every specimen. On both tables the results are sorted from the lowest examined value to the highest. Cracked specimens are marked with a (*).

Table 5.1: Solidification time and α coefficient of specimens

Specimen	Solidification time (s)	α
4	0.2362	0.194
11	0.2395	0.196
12*	0.2430	0.197
1	0.2480	0.199
5	0.2480	0.199
10*	0.2480	0.199
6*	0.2599	0.205
3*	0.2774	0.210

Table 5.2: Mushy zone size and heat input of specimens

Specimen	mushy zone size (mm^2)	heat input (J/mm)
4	8.069	98
11	8.128	108
1	8.933	103
5	8.933	103
10*	8.933	103
12*	9.168	122
6*	9.227	109
3*	9.855	117

It is interesting to notice that only the mushy zone model was able to give a better prediction regarding the specimens with the higher tendency for cracking. As it has been explained in [Fig 4.4], low values of α lead to a higher absolute value of hot cracking sensitivity index and results in higher tendency for cracking. However, in [Table 5.1] is easy to see that most of the specimens with the highest coefficient α exhibited cracks into their microstructure. A possible explanation is the fact that only one of the three factors mentioned in [Equation 2.6] has been taken into account. Moreover, the available specimens show small differences in their solidification time due to welding conditions and as a result there would not occur great differences on the susceptibility indexes. This statement does not mean that the other factors will also produce small changes. For instance, the different welding conditions lead to different thermal and stress fields that affect the left hand side term of [Equation 2.6].

On the other hand, the cracked specimens showed the widest mushy zones [Table 5.2]. As a result, the criterion that relates the crack tedency with the mushy zone size is accurate.

Chapter 6

Conclusions/Future work

6.1 Conclusions

Hot cracking in LBW of Aluminum alloy 2198 has been studied. Experimental and computational methods have contributed to the investigation. After reviewing the hot cracking mechanism and the factors that affect the tendency for cracks, two approaches were presented. The major conclusions are summarised hereinafter:

1)The microstructure prefers an isocolumnar formation in the outer region of the weld metal, whereas it prefers an equaxial formation in the inner region for all the examined specimens. Moreover particles of a Cu-rich phase nucleate on the grain boundaries.

2)The cracks propagate through the grain boundaries which characterise the hot cracking phenomenon. As a result the cracking mode is intergranural.

3)The specimens with heat input less that $103 J/mm$ seem to have a lower tendency for cracking.

4)The cracked grains have a tendency to be enriched in Cu on the interior, compared with the non-cracked grains. This confirms the proposed by Kou index which indicates a higher cracking tedency when refers to grains with higher Cu concentration on their interior.

5)The second phase particles found at the grain boundaries are composed mainly from Al and Cu with Cu concentration varying from 18.63% wt. to 38.15% wt. According to the literature this is an indication of the presence of θ (Al_2Cu) phase. It should be noted that due to the limitations arise from the characterization techniques employed in this study the Li consetration cannot be detected. In this context the participation of Li either in the solid solution or the secondary phases cannot be veryfied.

6) The mushy zone area has been calculated for all specimens. The results verify that the wider the mushy zone the higher the tendency for cracking. This is in agreement with the literature findings.

7)Despite the fact that the mushy zone model works well the proposed index by Kou failed to produce accurate predictions. A possible explanation is attributed to the fact that only one of the three factors mentioned in [Equation 2.6] has been taken into account. Moreover, the available specimens show small differences in their solidification time and as a result there would not occur great differences on the susceptibility indexes.

8) The best behaviour concerning hot cracking sensitivity has been observed in specimen 11, where a high heat input rate associated with small welding velocity and low laser power produced a small mushy zone and a crack free specimen.

9) In conclusion, for a crack free specimen the welding conditions should be selected in order to produce a small mushy zone (low laser power and low welding velocity) and small solidification time. This will constrain the non-equilibrium phenomena occuring during solidification.

6.2 Future work

Some suggestions for further research are the following:

1)Development of a multi-physics numeric mode which would calculate all the terms involved in Kou's Criterion [Equation 2.6]. Similar simulations have been already done for Al-Mg-Si alloys[10].

2)Calculation of the thermal field during welding with a more accurate model such as Finite Element Analysis. The aim should be to optimize the welding conditions aiming to minimize the mushy zone and as a result the tendency for cracking. Validation with experimental results.

3) Study of hot cracking behavior of aluminum alloy 2198 for Electron Beam Welding.

Bibliography

[1] JN DuPont. Mathematical modeling of solidification paths in ternary alloys: limiting cases of solute redistribution. *Metallurgical and Materials Transactions A*, 37(6):1937--1947, 2006.

[2] JN DuPont, AR Marder, MR Notis, and CV Robino. Solidification of nb-bearing superalloys: Part ii. pseudoternary solidification surfaces. *Metallurgical and Materials Transactions A*, 29(11):2797--2806, 1998.

[3] J Enz, C Carrarin, S Riekehr, V Ventzke, and N Kashaev. Hot cracking behaviour of an autogenously laser welded al-cu-li alloy. *The International Journal of Advanced Manufacturing Technology*, 95(1-4):299--310, 2018.

[4] Gregory N. Haidemenopoulos. *Physical Metallurgy*. Tziolas Publications, 2007.

[5] Gregory N. Haidemenopoulos. *Introduction in Welding Technology*. Tziolas Publications, 2010.

[6] Sindo Kou. A criterion for cracking during solidification. *Acta Materialia*, 88:366--374, 2015.

[7] Hong-ying Li, Xiong-jie Su, YIN Hao, and De-sheng Huang. Microstructural evolution during homogenization of al-cu-li-mn-zr-ti alloy. *Transactions of Nonferrous Metals Society of China*, 23(9):2543--2550, 2013.

[8] Jiangwei Liu and Sindo Kou. Susceptibility of ternary aluminum alloys to cracking during solidification. *Acta Materialia*, 125:513--523, 2017.

[9] N Eswara Prasad, Amol Gokhale, and RJH Wanhill. *Aluminum-lithium alloys: processing, properties, and applications*. Butterworth-Heinemann, 2013.

[10] HR Zareie Rajani and AB Phillion. 3d multi-scale multi-physics modelling of hot cracking in welding. *Materials & Design*, 144:45--54, 2018.

[11] Despoina Vriami. *Expiramental study of aeronautical aluminum alloys welding with high power beams (LBW,EBW)*. University of Thessaly-Department of Mechanical Engineering, 2010.

[12] S Yang, J Shen, X Yan, X Li, F Zhang, and B Sun. Homogenization treatment parameter optimization and microstructural evolution of al-cu-li alloy [j]. *Rare Metal Materials & Engineering*, 46(1):28--34, 2017.

[13] AD Zervaki, GN Haidemenopoulos, DP Vriami, and SG Lambrakos. Case-study inverse thermal analyses of al2198 laser welds. *Journal of materials engineering and performance*, 21(4):471--480, 2012.

[14] Sai-fei Zhang, Wei-dong Zeng, Wen-hua Yang, Chun-ling Shi, and Hao-jun Wang. Ageing response of a al--cu--li 2198 alloy. *Materials & Design*, 63:368--374, 2014.

[15] Zhixiong Zhu, Jian Han, Chong Gao, Mao Liu, Jianwei Song, Zhiwei Wang, and Huijun Li. Microstructures and mechanical properties of al-li 2198-t8 alloys processed by two different severe plastic deformation methods: A comparative study. *Materials Science and Engineering: A*, 681:65--73, 2017.